Table 4. Cases With the Same Pathogen Detected by Both Methods

Case/Sex/ Age, y	Pathogen Detected by Culture (Quantity)	Pathogen Detected by Real-Time PCR	DNA Copy No. (No. of Copies/Sample)	Smear Examination Results
1/16/F	*P aeruginosa* (≥3)	*P aeruginosa*	6.6×10^3	–
2/M/28	*P aeruginosa* (≥3)	*P aeruginosa*	9.4×10^2	GNR
3/M/19	*P aeruginosa* (≥2)	*P aeruginosa*	3.3×10^4	GNR
4/M/21	*P aeruginosa* (≥2)	*P aeruginosa*	3.2×10^3	–
5/F/78	*P aeruginosa* (≥1)	*P aeruginosa*	1.1×10^3	GNR
6/M/36	*P aeruginosa* (≥1)	*P aeruginosa*	1.6×10^3	GNR
7/M/22	*P aeruginosa* (≥1)	*P aeruginosa*	3.6×10^1	–
8/F/22	*P aeruginosa* (≥1)	*P aeruginosa*	4.5×10^1	–
9/M/61	*S pneumoniae* (≥5)	*S pneumoniae*	2.6×10^4	*Streptococcus*
10/M/79	*S pneumoniae* (≥2)	*S pneumoniae*	5.0×10^2	GPC
11/F/86	*S pneumoniae* (≥1)	*S pneumoniae*	2.6×10^2	–
12/F/16	*S pneumoniae* (≥1)	*S pneumoniae*	2.2×10^1	–
13/F/82	*S pneumoniae* (≥1)	*S pneumoniae*	1.0×10^3	–
14/M/54	*S aureus* (≥2)	*S aureus*	2.3×10^1	–
15/F/89	*S aureus* (≥2)	*S aureus*	6.4×10^1	–
16/F/63	*S aureus* (≥1)	*S aureus*	2.8×10^1	–
17/F/80	MRSA (≥3)	MRSA	1.0×10^2	GPC
18/F/80	*C albicans* (≥1)	*Candida* species	1.7×10^4	–
19/F/57	*Candida parapsilosis* (≥1)	*Candida* species	9.2×10^3	Yeast
20/F/54	*C albicans* (≥1)	*Candida* species	1.0×10^2	–

Abbreviations: *C albicans, Candida albicans*; GNR, gram-negative rods; GPC, gram-positive cocci; MRSA, methicillin-resistant *Staphylococcus aureus*; *P aeruginosa, Pseudomonas aeruginosa*; PCR, polymerase chain reaction; *S aureus, Staphylococcus aureus; S pneumoniae, Staphylococcus pneumoniae*; –, negative.

Table 5. Cases With Different Detection Results by Both Methods

Case/Sex/ Age, y	Pathogen Detected by Culture (Quantity)	Pathogen Detected by Real-Time PCR	DNA Copy No. (No. of Copies/Sample)	Smear Examination Results
21/F/29	*Acanthamoeba* (≥1)	MRSA	1.2×10^1	–
22/M/34	*Staphylococcus warneri* (≥1)	–		–
23/F/21	*Corynebacterium* species (≥1)	–		–
24/M/82	–	*P aeruginosa*	5.4×10^2	–
25/M/89	–	*P aeruginosa*	1.4×10^1	–
26/F/42	–	*P aeruginosa*	8.7×10^1	–
27/F/61	–	*S pneumoniae*	5.8×10^2	–
28/M/74	–	*S pneumoniae*	4.6×10^1	–
29/F/65	–	*S pneumoniae*	1.5×10^1	–
30/M/72	–	MRSA	1.3×10^2	–
31/F/72	–	MRSA	1.9×10^2	–
32/F/54	–	MRSA	1.2×10^1	–
33/F/79	–	*Candida* species	2.2×10^2	–
34/F/54	–	*Candida* species	8.5×10^2	–

Abbreviations: MRSA, methicillin-resistant *Staphylococcus aureus*; *P aeruginosa, Pseudomonas aeruginosa*; PCR, polymerase chain reaction; *S pneumoniae, Staphylococcus pneumoniae*; –, negative.

ods agreed in 26 eyes (20 eyes with matched pathogens and 6 eyes with negative results) (Tables 3 and 4) and disagreed in 14 eyes (11 eyes, positive PCR results only; 2 eyes, positive culture results only; and 1 eye, positive results for different pathogens) (Table 5). In the 2 eyes that had positive culture results only (cases 22 and 23) (Table 5), the detected pathogens (*Staphylococcus warneri* and *Corynebacterium* species) could not be detected by the real-time PCR assay because they were not included in the 6 target pathogens designed for the pathogen-specific probes and primers in this PCR study.

Among the matched pathogens in those 20 eyes, *P aeruginosa* was the most frequent pathogen (8 eyes; mean [SE], 5.1 [4.0] $\times 10^3$ copies/sample) and was followed by *S pneumoniae* (5 eyes; mean [SE], 5.6 [5.1] $\times 10^3$ copies/sample), *Candida* species (3 eyes; mean [SE], 8.8 [4.9] $\times 10^3$ copies/sample), *S aureus* (3 eyes; mean [SE], 3.8 [1.3] $\times 10^1$ copies/sample), and methicillin-resistant *S aureus* (1 eye; 1.0×10^2 copies/sample) (Table 4).

Of the 40 eyes, results of smear examination were positive in 8 eyes (20.0%) (Tables 4 and 5). This rate was low as compared with other reports,[5,27] because we dipped the swab into the culture media and applied it on the slide glass for smear examination.

SENSITIVITIES AND SPECIFICITIES OF REAL-TIME PCR FOR THE 6 PATHOGENS

By comparing the sensitivity and specificity of real-time PCR with those of bacterial and fungal culture, the rela-

tive sensitivities and specificities[5] of the real-time PCR assay for the 6 target pathogens were determined. A sensitivity of 100% was achieved for 5 pathogens of 6 and the relative specificities ranged from 89.7% to 100% (**Table 6**).

COMMENT

The current results obtained by culture method and real-time PCR coincided in 26 (65.0%) of the 40 eyes. Of those, 20 eyes had matched pathogens (Table 4) and the other 6 eyes showed negative results (Table 3) by both methods.

Accurate identification of causative organisms is essential to better management of corneal ulcer. A national surveillance[27] of infectious keratitis in Japan reported that 90% of cases of infectious keratitis are caused by bacteria and 10% are by fungi or *Acanthamoeba*. Approximately 50% of the bacterial pathogens are gram-positive cocci, such as the frequently occurring *S aureus, Staphylococcus epidermidis,* and *Streptococcus*, whereas *P aeruginosa* is the most prevalent pathogen among gram-negative bacilli, including *Moraxella* species, *Acinetobacter* species, and several other bacteria.[27] Furthermore, the US Centers for Disease Control and Prevention has issued a warning about increasing cases of *Fusarium* keratitis.[28] Multidrug-resistant pathogens and fungi have also been increasing because of improper use of antibiotics and steroids.[28] Based on the surveillance result, we designed the real-time PCR assay in this study for the 6 pathogens that are commonly detected in clinical ophthalmology and succeeded in simultaneous detection and quantification within 2 hours.

In our study, *P aeruginosa* was the most frequently detected pathogen and *S aureus* was the second. These results were a little different from those of other studies.[5,27] We think this is because almost all our cases were referrals from other clinics and many cases had been already treated by some antibiotics when they came to our hospital.

While the pathogen in 1 of the 3 cases with discrepant findings (cases 21-23) (Table 5) was thought to be *Acanthamoeba* (case 21) (Table 5), the other 2 cases (cases 22-23) were cured by multidrug therapy and the causative pathogen could not be verified. Eleven cases had positive PCR results only (2 fungal and 9 bacterial pathogens) (Table 5). Although PCR has a high risk of false positivity,[5,6] we actually treated the patients with positive PCR results only according to their real-time PCR results and the treatment outcomes were all satisfactory. This may demonstrate a better detection sensitivity in the PCR assay. Vengayil and colleagues[6] compared the results of PCR and the conventional microbiological techniques (gram smear, culture, and potassium hydroxide wet mount). They concluded that PCR is more efficient and sensitive than the conventional microbiological techniques in diagnosing fungal keratitis. Our current results of the 2 cases with positive PCR fungal pathogen results only agreed with their findings. In cases of patients pretreated with antibiotic therapy such as quinolone, the conventional culture is more likely to give false-negative results whereas real-time PCR may still show positivity. However, the high sensitivity of real-time PCR could lead to false-positive results. These can be caused by laboratory contamination from reagents and intrasample contamination.[6] In conclusion, not only culture results but also clinical symptoms, PCR findings, and conventional smear results should all be carefully considered to accurately determine the causative pathogen. Real-time PCR can be a fast diagnostic tool and may be useful as an adjunct to identify potential pathogens.[6]

Table 6. Sensitivities and Specificities of Real-Time PCR Compared With Those of Bacterial and Fungal Culture

Species and Real-Time PCR Result	No. of Samples (%) Also Showing Result by Culture		Total No. of Samples
	Positive	Negative	
Pseudomonas aeruginosa			
Positive	8 (100.0)	3 (9.4)	11
Negative	0	29 (90.6)	29
Total	**8**	**32**	**40**
Staphylococcus pneumoniae			
Positive	5 (100.0)	3 (8.6)	8
Negative	0	32 (91.4)	32
Total	**5**	**35**	**40**
MRSA			
Positive	1 (100.0)	4 (10.3)	5
Negative	0	35 (89.7)	35
Total	**1**	**39**	**40**
Staphylococcus aureus			
Positive	3 (100.0)	0	3
Negative	0	37 (100.0)	37
Total	**3**	**37**	**40**
Candida species			
Positive	3 (100.0)	2 (5.4)	5
Negative	0	35 (94.6)	35
Total	**3**	**37**	**40**
Fusarium species			
Positive	0	0	0
Negative	0	40 (100.0)	40
Total	**0**	**40**	**40**

Abbreviations: MRSA, methicillin-resistant *Staphylococcus aureus*; PCR, polymerase chain reaction.

Real-time PCR obtained high sensitivities (except *Fusarium* species) and specificities (89.7%-100%) for the 6 target pathogens against the gold standard culture technique (Table 6). A previous PCR study using a structured probe reported a sensitivity of 96.2% and a specificity of 93.2% for *S pneumoniae*,[13] and our results for *S pneumoniae* (100% and 89.7%) (Table 6) were comparable with the previous results. Kim and colleagues[5] reported that PCR is more sensitive to fungal than to bacterial pathogens. Because we had a small number of fungal cases in this study, a future study with a large number of bacterial and fungal cases can better validate the feasibility of the real-time PCR assay.

In conclusion, though the numbers included in this study were limited, particularly with fungal ulcers, we have demonstrated that real-time PCR can accurately and simultaneously detect bacterial and fungal pathogens in a speedy fashion. We targeted 6 pathogens this time. If the testing durations for the selected target pathogens are about the same, we suspect that theoretically it might be possible to simultaneously detect many bacterial and fungal pathogens in a single run. In the future, applications of the real-time PCR assay to more pathogens are of interest. We have already accomplished real-time PCR system for *Acanthamoeba* and *Aspergillus* species. With real-

time PCR, it may be possible to develop a diagnostic kit for pathogen-specific detection in the busy ophthalmic clinical practice.

Submitted for Publication: June 18, 2009; final revision received August 25, 2009; accepted September 4, 2009.
Correspondence: Shiro Higaki, MD, PhD, Department of Ophthalmology, Kinki University School of Medicine, 377-2 Ohno-Higashi, Osaka-Sayama 589-8511, Japan (higaki@ganka.med.kindai.ac.jp).
Financial Disclosure: None reported.
Additional Contributions: Mayumi Mizuno provided technical assistance.

REFERENCES

1. Schabereiter-Gurtner C, Maca S, Kaminsky S, Rölleke S, Lubitz W, Barisani-Asenbauer T. Investigation of an anaerobic microbial community associated with a corneal ulcer by denaturing gradient gel electrophoresis and 16S rDNA sequence analysis. *Diagn Microbiol Infect Dis.* 2002;43(3):193-199.
2. Rudolph T, Welinder-Olsson C, Lind-Brandberg L, Stenevi U. 16S rDNA PCR analysis of infectious keratitis: a case series. *Acta Ophthalmol Scand.* 2004;82(4):463-467.
3. Kumar M, Mishra NK, Shukla PK. Sensitive and rapid polymerase chain reaction based diagnosis of mycotic keratitis through single stranded conformation polymorphism. *Am J Ophthalmol.* 2005;140(5):851-857.
4. Gaudio PA, Gopinathan U, Sangwan V, Hughes TE. Polymerase chain reaction based detection of fungi in infected corneas. *Br J Ophthalmol.* 2002;86(7):755-760.
5. Kim E, Chidambaram JD, Srinivasan M, et al. Prospective comparison of microbial culture and polymerase chain reaction in the diagnosis of corneal ulcer. *Am J Ophthalmol.* 2008;146(5):714-723, 723, e1.
6. Vengayil S, Panda A, Satpathy G, et al. Polymerase chain reaction-guided diagnosis of mycotic keratitis: a prospective evaluation of its efficacy and limitations. *Invest Ophthalmol Vis Sci.* 2009;50(1):152-156.
7. Kaufman HE, Azcuy AM, Varnell ED, Sloop GD, Thompson HW, Hill JM. HSV-1 DNA in tears and saliva of normal adults. *Invest Ophthalmol Vis Sci.* 2005;46(1):241-247.
8. Fukuda M, Deai T, Hibino T, Higaki S, Hayashi K, Shimomura Y. Quantitative analysis of herpes simplex virus genome in tears from patients with herpetic keratitis. *Cornea.* 2003;22(7)(suppl):S55-S60.
9. Itahashi M, Higaki S, Shimomura Y. Effects of anti herpetic drugs on mice with herpetic epithelial keratitis after reactivation of herpes simplex virus type 1. *Semin Ophthalmol.* 2008;23(4):241-247.
10. Higaki S, Itahashi M, Deai T, Fukuda M, Shimomura Y. Effect of oral valacyclovir on herpetic keratitis. *Cornea.* 2006;25(10)(suppl 1):S64-S67.
11. Zhang Y, Kimura T, Fujiki K, Sakuma H, Murakami A, Kanai A. Multiplex polymerase chain reaction for detection of herpes simplex virus type 1, type 2, cytomegalovirus, and varicella-zoster virus in ocular viral infections. *Jpn J Ophthalmol.* 2003;47(3):260-264.
12. Weidmann M, Meyer-König U, Hufert FT. Rapid detection of herpes simplex virus and varicella-zoster virus infections by real-time PCR. *J Clin Microbiol.* 2003;41(4):1565-1568.
13. Morozumi M, Nakayama E, Iwata S, et al. Simultaneous detection of pathogens in clinical samples from patients with community-acquired pneumonia by real-time PCR with pathogen-specific molecular beacon probes. *J Clin Microbiol.* 2006;44(4):1440-1446.
14. Duck P, Alvarado-Urbina G, Burdick B, Collier B. Probe amplifier system based on chimeric cycling oligonucleotides. *Biotechniques.* 1990;9(2):142-148.
15. Hogrefe HH, Hogrefe RI, Walder RY, Walder JA. Kinetic analysis of *Escherichia coli* RNase H using DNA-RNA-DNA/DNA substrates. *J Biol Chem.* 1990;265(10):5561-5566.
16. Yabutani M, Agata N, Ohta M. A new rapid and sensitive detection method for cereulide-producing *Bacillus cereus* using a Cycleave real-time PCR. *Lett Appl Microbiol.* 2009;48(6):698-704.
17. Modrusan Z, Bekkaoui F, Duck P. Spermine-mediated improvement of cycling probe reaction. *Mol Cell Probes.* 1998;12(2):107-116.
18. Bekkaoui F, Poisson I, Crosby W, Cloney L, Duck P. Cycling probe technology with RNase H attached to an oligonucleotide. *Biotechniques.* 1996;20(2):240-248.
19. Zucol F, Ammann RA, Berger C, et al. Real-time quantitative broad-range PCR assay for detection of the 16S rRNA gene followed by sequencing for species identification. *J Clin Microbiol.* 2006;44(8):2750-2759.
20. Kobayashi N, Bauer TW, Togawa D, et al. A molecular gram stain using broad range PCR and pyrosequencing technology: a potentially useful tool for diagnosing orthopaedic infections. *Diagn Mol Pathol.* 2005;14(2):83-89.
21. Sau S, Bhasin N, Wann ER, Lee JC, Foster TJ, Lee CY. The *Staphylococcus aureus* allelic genetic loci for serotype 5 and 8 capsule expression contain the type-specific genes flanked by common genes. *Microbiology.* 1997;143(pt 7):2395-2405.
22. Motoshima M, Yanagihara K, Fukushima K, et al. Rapid and accurate detection of *Pseudomonas aeruginosa* by real-time polymerase chain reaction with melting curve analysis targeting gyrB gene. *Diagn Microbiol Infect Dis.* 2007;58(1):53-58.
23. Francois P, Pittet D, Bento M, et al. Rapid detection of methicillin-resistant *Staphylococcus aureus* directly from sterile or nonsterile clinical samples by a new molecular assay. *J Clin Microbiol.* 2003;41(1):254-260.
24. Bekkaoui F, McNevin JP, Leung CH, et al. Rapid detection of the mecA gene in methicillin resistant staphylococci using a colorimetric cycling probe technology. *Diagn Microbiol Infect Dis.* 1999;34(2):83-90.
25. Kasai M, Francesconi A, Petraitiene R, et al. Use of quantitative real-time PCR to study the kinetics of extracellular DNA released from *Candida albicans*, with implications for diagnosis of invasive *Candidiasis. J Clin Microbiol.* 2006;44(1):143-150.
26. Filion M, St-Arnaud M, Jabaji-Hare SH. Direct quantification of fungal DNA from soil substrate using real-time PCR. *J Microbiol Methods.* 2003;53(1):67-76.
27. Study Group of National Surveillance of Infectious Keratitis in Japan. National surveillance of infectious keratitis in Japan. *J Jpn Ophthalmol Soc.* 2006;110(12):961-972.
28. Chang DC, Grant GB, O'Donnell K, et al; *Fusarium* Keratitis Investigation Team. Multistate outbreak of *Fusarium* keratitis associated with use of a contact lens solution. *JAMA.* 2006;296(8):953-963.

Jpn J Ophthalmol 2010;54:32–35
DOI 10.1007/s10384-009-0752-x

CLINICAL INVESTIGATION

Oscillatory Potentials with Repeated-Flash Electroretinography

Kazuki Kuniyoshi, Motohiro Irifune, Naoki Uno, Akira Nakao, and Yoshikazu Shimomura

Department of Ophthalmology, Kinki University School of Medicine, Osaka, Japan

Abstract

Purpose: To study the influence of retinal adaptation on oscillatory potential (OP) using repeated-flash electroretinography.

Methods: Subjects were 28 adult eyes with normal retinas. Four stimuli (four flashes) of white light from a light-emitting diode built into a contact lens that also served as the recording electrode were presented at 5-s intervals after 30 min of dark adaptation (DA) and then after 10 min of light adaptation (LA). Recordings were made without background light.

Results: Four OPs (O1, O2, O3, and O4) were recordable. After DA, amplitudes of O1 and O4 decreased with subsequent flashes, whereas those of O2 increased after the second flash. After LA, amplitudes of O3 and O4 were smaller than after DA.

Conclusions: Amplitude and implicit time of OPs were influenced by retinal adaptation. Among all OPs, O2 showed unique characteristics in course of retinal adaptation. **Jpn J Ophthalmol** 2010;54:32–35

Keywords: dark adaptation, electroretinogram, light adaptation, oscillatory potentials, repeated-flash ERG

Introduction

Repeated-flash (double-flash) electroretinography (ERG) has been used to study retinal function in normal subjects[1–9] and in patients with various retinal diseases.[10–15] Most of repeated-flash ERG investigations have analyzed a and b waves, although some[1–7] have observed the behavior of oscillatory potentials (OPs), which appear on the ascending portion of the b wave as a series of small wavelets.

Amplitude and implicit time of OPs are influenced by retinal adaptation.[16–19] The aim of this paper is to examine the ways in which retinal adaptation influences the behavior of OPs using repeated-flash stimuli.

Received: March 24, 2009 / Accepted: August 31, 2009
Correspondence and reprint requests to: Kazuki Kuniyoshi, Department of Ophthalmology, Kinki University School of Medicine, 377-2 Ohno-Higashi, Osaka-Sayama, Osaka 589-8511, Japan
e-mail: kuniyoshi@ganka.med.kindai.ac.jp

Subjects and Methods

Subjects for this study were 28 eyes of 28 individuals (median age, 40 years; range, 19–62 years) with no retinal disease. The research followed the tenets of the Declaration of Helsinki. All subjects gave written informed consent to participate in the study.

Repeated-flash electroretinograms were recorded after both dark and light adaptation, and consecutive changes of OPs were observed using repeated-flash stimuli under both dark and light adaptation.

Electroretinograms were recorded by using a contact lens with a built-in light-emitting diode (LED) that served both as the stimulus light source (connected to a constant-current source) and as the active recording electrode (LED electrode) (WLS-20, Tomey, Nagoya, Japan). A four-channel amplifier (MEB-5504, Nihonkohden, Tokyo, Japan) was used to record ERG responses and OPs separately.

All ERG examinations were performed in a wire-net shielded room. The pupils were dilated to more than 8 mm

in diameter with 0.5% tropicamide and 0.5% phenylephrine hydrochloride. After a 30-min period of dark adaptation, the LED electrode was placed on the cornea. A reference electrode was placed at the center of the forehead, and a ground electrode was placed on an earlobe.

Dark-adapted flash electroretinograms were recorded in response to four flashes (first flash, second flash, etc.) with an interval of 5 s between flashes. Each flash had a luminance of 6000 cd/m^2 and a duration of 5 ms (30 cd-s/m^2). The recorded responses were band-pass filtered from 0.1 to 1000 Hz for a and b waves, and from 100 to 1000 Hz for OPs alone. The notch filter was excluded from the amplifier circuit.

After dark-adaptation recording, the retina was light-adapted by exposure for 10 min to background light of 80 cd/m^2. The background light was extinguished, and flash ERGs and OPs were recorded again in the same manner as after dark adaptation, and the responses were filtered using the same filter settings.

Results

Results are shown in Figs. 1 to 7. After dark adaptation, the mean amplitudes of the first (O1) and fourth (O4) OP gradually decreased from the first flash to the fourth flash, whereas the amplitude of the second OP (O2) increased in response to the second flash and then decreased somewhat in response to the third and fourth flashes (Figs. 1–4). The amplitude of the third OP (O3) varied among subjects. In ten subjects, the amplitude of O3 was greater (by more than 1.5 times) in response to the second flash than that in response to the first flash after dark adaptation (Fig. 2), whereas in five subjects the amplitude of O3 decreased with each subsequent flash (Fig. 3).

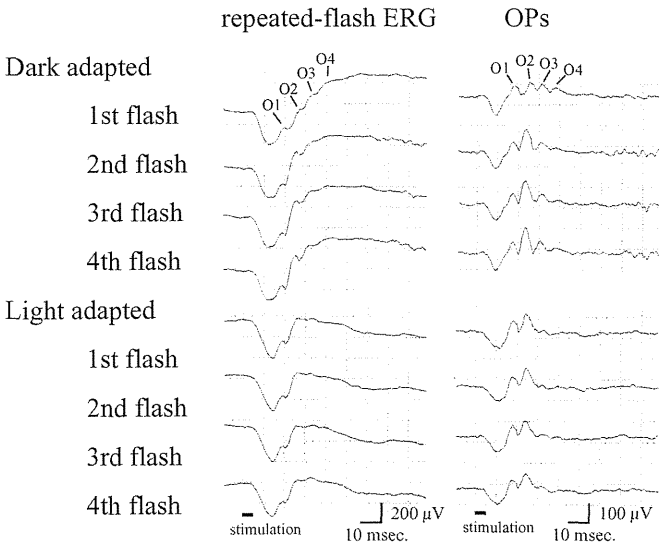

Figure 1. Repeated-flash electroretinograms (*ERGs, left column*) and oscillatory potentials (*OPs*) alone (*right column*) recorded in a normal subject after 30 min of dark adaptation (*Dark adapted*) and after 10 min of light adaptation (*Light adapted*). *O1*, *O2*, *O3*, and *O4* indicate the first, second, third, and fourth OP. After dark adaptation, O2 increased in amplitude and decreased in peak time in response to each successive (second, third, and fourth) flash.

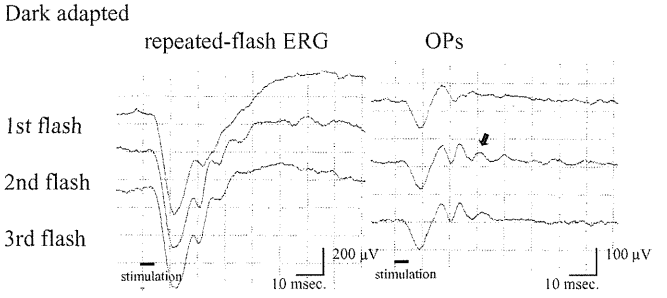

Figure 2. Repeated-flash ERGs (*left column*) and OPs alone (*right column*) in a normal subject after 30 min of dark adaptation. In this subject, the amplitude of O3 increased with each repetition of the flash (*arrow*).

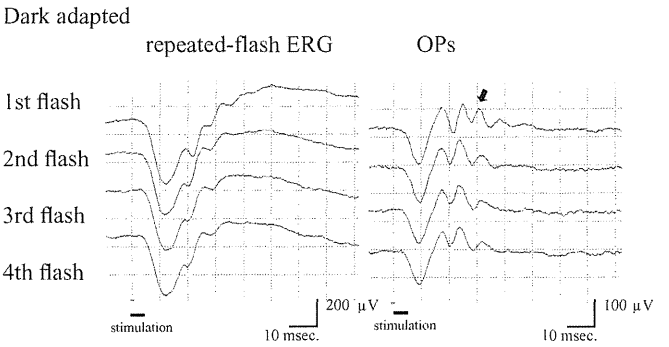

Figure 3. Repeated-flash ERGs (*left column*) and OPs alone (*right column*) in a normal subject after 30 min of dark adaptation. In this subject, O3 decreased in amplitude with each repetition of the flash (*arrow*).

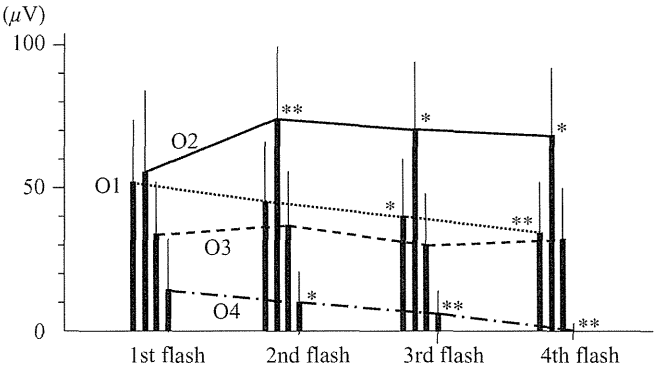

Figure 4. Mean amplitudes of O1, O2, O3, and O4 recorded in 28 normal subjects in response to repeated-flash stimuli (*1st flash*, etc.) after a 30-min period of dark adaptation. On repetition of the flash stimulus, the amplitudes of O1 and O4 decreased significantly (P = 0.0175 and 0.00525 for O1; P = 0.0424, 0.0026, and 0.00002 for O4), but the amplitude of O2 increased significantly (P = 0.00565, 0.0202, and 0.0377). $^*P < 0.05$; $^{**}P < 0.01$ versus 1st-flash ERG.

Jpn J Ophthalmol
Vol 54: 32–35, 2010

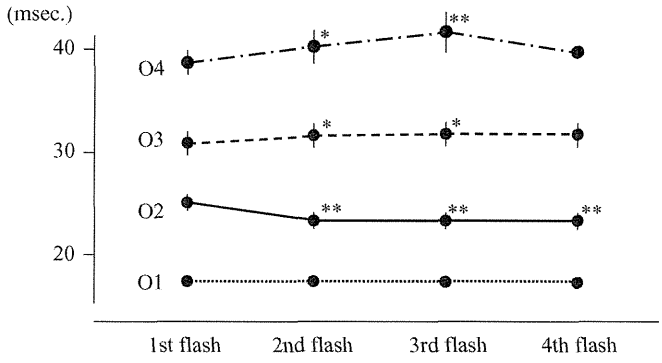

Figure 5. Mean peak times of O1, O2, O3, and O4 recorded in 28 normal subjects in response to repeated-flash stimuli (*1st flash*, etc.) after 30 min of dark adaptation. Repetition of the flash stimulus resulted in significant decrease in peak time of O2 (P = 0.000058, 0.0000076, and 0.000043), but increases in peak times of O3 and O4 (P = 0.0431 and 0.0145 for O3; P = 0.0400 and 0.00381 for O4). $^{*}P < 0.05$; $^{**}P < 0.01$ versus 1st-flash ERG.

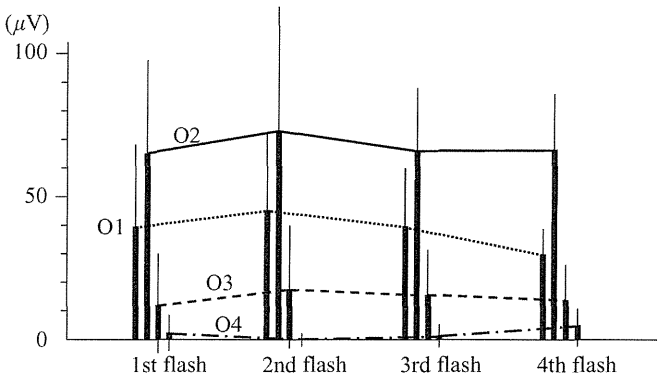

Figure 6. Mean amplitudes of O1, O2, O3, and O4 recorded in 28 normal subjects in response to repeated-flash stimuli (*1st flash*, etc.) after 10 min of light adaptation. Repetition of the flash stimulus did not result in any significant change in amplitude.

The peak time of O1 did not change significantly with repetition of the flash stimulus, but the peak time of O2 decreased significantly for the second, third, and fourth flashes compared with the first flash (Figs. 1, 3, and 5). The peak times of O3 and O4 were significantly longer in response to the second and third flashes, but not in response to the fourth flash, compared with the first flash (Fig. 5).

After light adaptation, the amplitudes and peak times of all four OPs did not vary in response to repeated flashes (Fig. 1), and none of the differences were significant compared with the first flash (Figs. 6 and 7). The amplitudes of O3 and O4 recorded after light adaptation were much smaller than those of O3 and O4 recorded after dark adaptation (Figs. 4 and 6).

Discussion

Although OPs were discovered about 60 years ago,[20,21] their origins are still unclear. The results of animal experiments

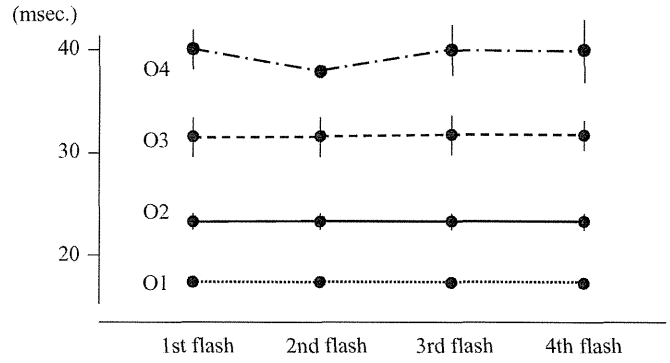

Figure 7. Mean peak times of O1, O2, O3, and O4 recorded in 28 normal subjects in response to repeated-flash stimuli (*1st flash*, etc.) after 10 min of light adaptation. Repetition of the flash stimulus resulted in no significant change in peak times.

indicate that OPs may arise in bipolar cells,[22,23] in amacrine cells,[24] or in the inner plexiform layer of the retina.[25–27] Wachtmeister and Dowling[26] contributed to the knowledge of OPs by demonstrating that OPs reverse polarity in different layers of the retina and that the first OP (O1) reverses polarity at the border between the inner plexiform layer and the inner nuclear layer, more proximally than the other OPs. They proposed that OPs result from radial electrical flows in the retina. King-Smith and colleagues[28] recorded OPs separately from cone and rod systems and found that OPs originating from cone systems have shorter peak time than those originating from rod systems.

Many investigators have studied differences in OPs recorded under either scotopic or photopic conditions,[16–19,29–33] recorded in response to light stimuli of various colors,[28,34–36] or by using various locations of the active electrode.[37] The findings of some of these studies[18,32,36] suggest that O1 and O2 are generated mostly by cone systems and O3 and O4 mostly by rod systems. Tremblay and Lam[37] reported that the point of inversion of polarity is similar for O2 and O3 but different for O4. The findings of these studies suggest that both rod and cone systems may contribute to the generation of OPs, although each OP is generated by a unique combination of retinal components.

We recorded OPs both after 30 min of dark adaptation and after 10 min of light adaptation using repeated high-intensity flash stimuli with an interval of 5 s between stimuli. Under these conditions, the obtained electroretinograms contain both rod- and cone-driven responses. As a result, the reaction of OPs to the consecutive flash stimuli varied for O1, O2, O3 and O4.

O1 was recordable under both dark- and light-adapted conditions. On the other hand, though O3 and O4 were recordable with every stimulus under dark adaptation, they almost entirely disappeared after light adaptation (Figs. 1, 4, and 6). These results support the hypothesis that O1 is generated mostly by cone systems and O3 and O4 mostly by rod systems.[18,32,36]

The reaction of O2 to repeated-flash stimuli was unique among OPs. The striking characteristic of O2 was that its

amplitude was larger and peak time was shorter with the second and later flash stimuli. In other words, the O2 elicited by the first flash was different from the other O2s in both amplitude and peak time. These findings indicate that O2 is the most sensitive to the retinal condition (i.e., adaptation level of the retina) among the OPs.

Irifune[38] examined OPs in patients with diabetes and found abnormalities of OPs even in diabetic patients without diabetic retinopathy, concluding that these abnormalities may be enhanced by disturbances in dark adaptation in the early stages of diabetes. In the clinic, OPs recorded from an affected retina should be evaluated with care, because disturbances of either light or dark adaptation of the retina may influence the amplitude or peak time of OPs.

In conclusion, OPs were influenced by retinal adaptation. O1 was the least influenced by both the repeated flashes and light adaptation. O3 and O4 were easily attenuated with repetition of either flash stimuli or light adaptation. O2 was unique among OPs because the preceding flash or subtle light adaptation made the amplitude bigger and the peak time shorter.

References

1. Dodt E. Beiträge zur Elektrophysiologie des Auges. II. Mitteilung. Über Hemmungsvorgänge in der menschlichen Retina. Graefes Arch Ophthalmol 1952;153:152–162.
2. Mahneke A. Electroretinography with double flashes. Acta Ophthalmol 1957;35:131–141.
3. Burian HM, Spivey BE. The effect of twin flashes and of repetitive light stimuli on the human electroretinogram. Am J Ophthalmol 1959;48:274–286.
4. Algvere P, Westbeck S. Human ERG in response to double flashes of light during the course of dark adaptation: a Fourier analysis of the oscillatory potentials. Vision Res 1972;12:195–214.
5. Algvere P, Wachtmeister L, Westbeck S. On the oscillatory potentials of the human electroretinogram in light and dark adaptation. I. Thresholds and relation to stimulus intensity on adaptation to short flashes of light. A Fourier analysis. Acta Ophthalmol 1972;50:737–759.
6. Wachtmeister L. On the oscillatory potentials of the human electroretinogram in light and dark adaptation. IV. Effect of adaptation to short flashes of light. Time interval and intensity of conditioning flashes. A Fourier analysis. Acta Ophthalmol 1972; 50:250–269.
7. Gjötterberg M. Double flash human electroretinogram with special reference to the oscillatory potentials and the early phase of dark adaptation: a normative study. Acta Ophthalmol 1974;52: 291–304.
8. Kooijman AC, Zwarts J, Damhof A. Double-flash electroretinography in human eyes. Doc Ophthalmol 1990;73:377–385.
9. Saeki M, Gouras P. Cone ERGs to flash trains: the antagonism of a later flash. Vision Res 1996;36:3229–3235.
10. Bornschein H, Gunter R. The double-flash ERG in retinal ischemia. Vision Res 1964;4:423–432.
11. Elenius V. Double-flash ERG in central serous retinopathy. Acta Ophthalmol 1968;46:976–979.
12. Gliem H, Möller DE, Kietzmann G. Das Doppelblitz-ERG bei der diabetischen Retinopathie. Acta Ophthalmol 1973;51:85–94.
13. Mitsuyu M, Honda Y, Negi A. Application of twin flash stimuli for some macular diseases. Isolation of local responses by twin flashes. Acta Ophthalmol 1980;58:688–696.
14. Peachey NS, Alexander KR, Fishman GA. Rod and cone system contributions to oscillatory potentials: an explanation for the conditioning flash effect. Vision Res 1987;27:859–866.
15. Bartz-Schmidt KU, Brunner R, Esser P, Lüke C, Walter P, Sickel W. The triple flash electroretinogram and its significance in macular diseases. B-wave recovery as a diagnostic tool. Graefes Arch Clin Exp Ophthalmol 1996;234:604–611.
16. DeMolfetta V, Spinelli D, Polenghi F. Behavior of electroretinographic oscillatory potentials during adaptation to darkness. Arch Ophthalmol 1968;79:531–535.
17. Wachtmeister L. On the oscillatory potentials of the human electroretinogram in light and dark adaptation. Acta Ophthalmol suppl. 1972;116:1–32.
18. Rousseau S, Lachapelle P. The electroretinogram recorded at the onset of dark-adaptation: understanding the origin of the scotopic oscillatory potentials. Doc Ophthalmol 1999;99:135–150.
19. Kuze M, Uji Y. Changes in electroretinogram oscillatory potentials during dark adaptation. Jpn J Ophthalmol 2005;49:420–422.
20. Granit R, Munsterhjelm A. The electrical responses of dark adapted frogs' eyes to monochromatic stimuli. J Physiol 1937;88: 436–458.
21. Cobb WA, Morton HB. A new component of the human electroretinogram. J Physiol 1954;123 suppl.:36–37.
22. Yonemura D, Hatta M. Studies of the minor components of the frog's electroretinogram. Jpn J Physiol 1966;16:11–22.
23. Heynen H, Wachtmeister L, van Norren D. Origin of the oscillatory potentials in the primate retina. Vision Res 1985;25:1365–1373.
24. Korol S, Leuenberger PM, Englert U, Babel J. *In vivo* effects of glycine on retinal ultrastructure and averaged electroretinogram. Brain Res 1975;97:235–251.
25. Ogden TE. The oscillatory waves of the primate electroretinogram. Vision Res 1973;13:1059–1074.
26. Wachtmeister L, Dowling JE. The oscillatory potentials of the mudpuppy retina. Invest Ophthalmol Vis Sci 1978;17:1176–1188.
27. Yanagida T, Koshimizu M, Kawasaki K, Yonemura D. Microelectrode depth study of the electroretinographic oscillatory potentials in the frog retina. Doc Ophthalmol 1988;67:355–361.
28. King-Smith PE, Loffing DH, Jones R. Rod and cone ERGs and their oscillatory potentials. Invest Ophthalmol Vis Sci 1986;27: 270–273.
29. Genest AA. Oscillatory potentials in the electroretinogram of the normal human eye. Vision Res 1964;4:595–604.
30. Algvere P, Wachtmeister L. On the oscillatory potentials of the human electroretinogram in light and dark adaptation. II. Effect of adaptation to background light and subsequent recovery in the dark. A Fourier analysis. Acta Ophtalmol 1972;50:837–862.
31. Wachtmeister L. On the oscillatory potentials of the human electroretinogram in light and dark adaptation. III. Thresholds and relation to stimulus intensity on adaptation to background light. Acta Ophtalmol 1973;51:95–113.
32. Coupland SG. Oscillatory potential changes related to stimulus intensity and light adaptation. Doc Ophthalmol 1987;66:195–205.
33. Peachey NS, Alexander KR, Derlacki DJ, Bobak P, Fishman GA. Effects of light adaptation on the response characteristics of human oscillatory potentials. Electroencephalogr Clin Neurophysiol 1991;78:27–34.
34. Wachtmeister L. Luminosity functions of the oscillatory potentials of the human electroretinogram. Acta Ophthalmol 1974;52: 353–366.
35. Wachtmeister L. Incremental thresholds of the oscillatory potentials of the human electroretinogram in response to coloured light. Acta Ophthalmol 1974;52:378–389.
36. Janáky M, Goupland SG, Benedek G. Human oscillatory potentials: components of rod origin. Ophthalmologica 1996;210: 315–318.
37. Tremblay F, Lam SR. Distinct electroretinographic oscillatory potential generators as revealed by field distribution. Doc Ophthalmol 1993;84:279–289.
38. Irifune M. Evaluation of ERGs recorded in patients with diabetic retinopathy and maculopathy. Med J Kinki Univ 2002;27: 149–163.

Role of Periostin and Interleukin-4 in Recurrence of Pterygia

Chuan-Hui Kuo,[1] *Dai Miyazaki,*[1] *Keiko Yakura,*[1] *Kaoru Araki-Sasaki,*[2] *and Yoshitsugu Inoue*[1]

Purpose. To identify the candidate genes for pterygia recurrence from a pterygia transcriptome and to analyze their transcriptional regulation and functional relationships.

Methods. Transcriptional networks for pterygia recurrence were constructed using network analysis that was applied to 184 genes that showed a significant twofold change in the whole genome. Of the identified recurrence-related candidate genes in the major networks, periostin and IL-4 were analyzed for transcriptional relationships using pterygia-derived fibroblasts. Immunohistochemical analysis was used to study pterygia tissue. Effector candidate molecule for recurrence periostin was analyzed for cell adhesive function.

Results. The pterygia transcriptome was divided into four major biological networks with high significance scores ($P < 10^{-17}$). The classifier with the highest accuracy using the support vector machine algorithm was periostin, which was successfully linked to the network of cell cycle, connective tissue development and function, and cell morphology. Analyses using pterygia-derived fibroblasts showed that periostin was required for cell adhesion that was mediated by a presumed pterygia-related extracellular matrix protein, fibronectin. Periostin was found to be transcriptionally induced by IL-4. The IL-4-stimulated periostin induction was suppressed by MAP kinase/ERK kinase 1 inhibitor, indicating an involvement of the MAP kinase pathway. Pathologically, IL-4 was transcriptionally elevated in recurrent pterygia tissue and was localized to perivascular tissues and endothelial cells in the stroma of the subconjunctiva of pterygia.

Conclusions. Periostin is induced by IL-4 and is involved in the fibronectin-mediated pterygia fibroblast adhesion. These findings indicate that periostin probably promotes the recurrence of pterygia. (*Invest Ophthalmol Vis Sci.* 2010;51:139-143) DOI:10.1167/iovs.09-4022

A pterygium is an excessive fibrovascular proliferation of degenerated bulbar conjunctival tissue on the ocular surface. At present, surgery is the only method for treating pterygia, and recurrences are a major complication of the surgical treatment of pterygia. Although numerous approaches have been attempted to reduce recurrences, such as adjunctive mitomycin treatment, radiation, and amniotic membrane transplantation, recurrences still occur.[1]

We have determined the minimum gene set that would accurately differentiate primary from recurrent pterygia using a mathematical classification algorithm.[2] We found that only three genes—periostin, tissue inhibitor of metalloproteinases-2 (TIMP-2), and l-3-phosphoserine phosphatase homolog (PSPHL)—differentiate primary from recurrent pterygia.[2]

We have also reported on the numerous transcripts that are related to pterygia recurrence.[2] However, the functional involvement in the genome or their significance in recurrence remains speculative. We have used knowledge-based analysis to understand the global interactions of the genes in the context of their function and regulation. To simplify the complex biological phenomena played by genes, network analysis has been reported to be a very efficient method.[3] We have applied the Ingenuity Pathways Knowledge Base (Ingenuity Systems, Redwood City, CA, http://www.ingenuity.com), a biological network database created from known protein-protein interactions and the activation of signaling pathways, and found that the complex phenomena of pterygia recurrences can be simply summarized into four highly significant molecular networks. In this analyses, periostin and TIMP-2, which we reported as significant classifier genes in the support vector machine (SVM)-based classification algorithm,[2] were statistically linked to the generated networks. Previously, TIMP-2 was shown to be involved in tissue remodeling processes of pterygia.[1] Although periostin showed the highest classification accuracies of primary and recurrent pterygia,[2] its functional characteristics are not yet well understood, and its involvement in the pathogenesis of pterygia has not been reported.

Thus, the purpose of this study was to determine the molecular function of periostin in pterygia pathology and the causative transcriptional event for periostin induction based on the generated networks. We shall show the function of periostin in the recurrence of pterygia and relate it to the role of IL-4 as its inductive signal.

Materials and Methods

Patient Backgrounds and Specimen Collection

Pterygia heads were collected from 21 eyes of 21 Asian patients undergoing pterygium excision with conjunctival autografting at the Tottori University Hospital (Yonago, Japan) and the Ideta Eye Hospital (Kumamoto, Japan). Of these, 11 eyes of 11 patients showed primary pterygia and 10 eyes of 10 patients showed recurrent pterygia. Patients were 11 men and 10 women whose mean age was 68 ± 2 years (range, 52-85 years). Patients with primary cicatricial ocular surface disease, history of ocular allergic symptoms, and inflammatory ocular surface disease of unknown etiology were excluded. The study protocol conformed to the tenets of the Declaration of Helsinki, and the procedures used were approved by the Tottori University Ethics Committee. Signed informed consent was obtained from all patients.

From the [1]Division of Ophthalmology and Visual Science, Tottori University Faculty of Medicine, Tottori, Japan; and [2]Ideta Eye Hospital, Kumamoto, Japan.

Supported by Grant-in-Aid for Scientific Research (C) 21592258 from the Ministry of Education, Culture, Sports, Science and Technology.

Submitted for publication May 21, 2009; revised July 1, 2009; accepted July 21, 2009.

Disclosure: **C.-H. Kuo**, None; **D. Miyazaki**, None; **K. Yakura**, None; **K. Araki-Sasaki**, None; **Y. Inoue**, None

Corresponding author: Dai Miyazaki, Division of Ophthalmology and Visual Science, Tottori University Faculty of Medicine, 36-1 Nishicho, Yonago Tottori 683-8504, Japan; dm@grape.med.tottori-u.ac.jp.

Transcriptional Analysis

Pterygia head tissues collected from primary and recurrence cases were transcriptionally analyzed using an oligo microarray (AceGene, Hitachi, Japan) corresponding to 30,336 human genes.[2] Genes that were differentially induced or suppressed in the primary and recurrent pterygia cases were extracted from the whole genome using *t* tests. This set of genes was analyzed using a bioinformatics approach.

To gain insight into the transcriptional network of molecular events in terms of the mechanism of recurrence, we applied commercially available analysis software (Ingenuity Pathway Analysis 3.0, based on the Ingenuity Pathways Knowledge Base; Ingenuity Systems, Redwood City, CA; http://www.ingenuity.com). The resultant networks were evaluated by the significance score, which is expressed as the negative logarithm of that *P*-value. The obtained score in each instance indicated the likelihood that the assembly of a set of focus genes in a network could be explained by random chance alone.

Real-Time RT-PCR

Total RNA was isolated from the treated fibroblasts using a purification kit (RNeasy Mini Kit; Qiagen, Hilden, Germany) according to the manufacturer's protocol. One microgram of RNA samples was reverse transcribed using random hexamers and superscript III (Invitrogen, Carlsbad, CA). The cDNAs were amplified and quantified (LightCycler; Roche, Mannheim, Germany) with a one-step quantification of RNA kit (QuantiTect SYBR Green PCR kit; Qiagen). Sequences of the used real-time PCR primer pairs were as follows: IL-4: forward, 5′-CACCGAGTTGACCGTAACAG-3′; reverse, 5′- GCCCTGCAGAAGGTTTCC-3′; periostin: forward, 5′-TTGAGACGCTGGAAGGAAAT-3′; reverse, 5′-AGATCCGTGAAGGTGGTTTG-3′; *IL-13:* forward, 5′-*TGGAGGACTTCTAGGAAAACGA-3′*; reverse, 5′-*CCCCTTTGCTCACCAGTCT-3′*; glyceraldehyde-3-phosphate dehydrogenase (GAPDH): forward, 5′-AGCCACATCGCTCAGACAC-3′; reverse, 5′-GCCCAATACGACCAAATCC-3′.

To ensure equal loading and amplification, all products were normalized to GAPDH transcript as an internal control.

Establishment of Pterygia Tissue–Derived Fibroblast Line

Head tissues of pterygia were collected from four eyes of four patients without a history of pterygia surgery and were undergoing primary excision with conjunctival autografting at the Tottori University Hospital. Tissues were minced using a sterilized forceps and scissors and digested in 12.5 mg/mL collagenase (Nitta Gelatin, Osaka, Japan) at 37°C in a humidified atmosphere of 5% CO_2 for 1 hour. The digested tissue was filtered and washed by centrifugation at 1500 rpm for 5 minutes and was cultured in Dulbecco's modified Eagle's medium (DMEM; Gibco-BRL, Carlsbad, CA) supplemented with 15% FBS (vol/vol) at 37°C in 5% CO_2. The pterygia-derived conjunctival fibroblasts were cultured to at least the third passage before use.

Fibroblast Adhesion Assay

An adhesion assay was performed as described.[4] Briefly, flat-bottom cell culture plates (Corning Costar, Cambridge, MA) were coated with 0 to 40 μg/mL purified human fibronectin (Gibco-BRL) in PBS at 4°C overnight. The plates were washed three times with PBS and blocked with 10 μg/mL heat-denatured bovine serum albumin (BSA; 85°C for 15 minutes; Sigma, St. Louis, MO) for 1 hour at 37°C. After blocking, the plates were washed with DMEM.

Fibroblasts, detached by enzyme treatment (Accutase; Innovative Cell Technologies, San Diego, CA), were incubated in DMEM for 30 minutes at 37°C in a tube rotator. The cells were then incubated in 0.1% BSA/PBS with antiperiostin (rabbit polyclonal antibody; 1:500; Biovendor, Brno, Czech Republic) or control IgG for 30 minutes at 4°C. After washing, the fibroblasts were seeded on fibronectin-coated plates (5×10^5 cells/well) in DMEM containing 1 μg/mL antiperiostin or control antibody and were incubated at 37°C for 1 hour. The medium was aspirated, and the plates were washed with PBS three times. The number of attached fibroblast was determined by dye (CyQUANT GR; Molecular Probes Inc., Eugene, OR) according to the manufacturer's protocol. Briefly, the solution (CyQUANT GR; Molecular Probes Inc.) was added to each well, and the fluorescence of the samples was measured at 520 nm with excitation at 480 nm fluorescence microplate reader (FL600; BioTek Instruments, Winooski, VT). Cell counts were calculated based on the calibration curve of fluorescence of diluted cell suspension.

Evaluation of Periostin Expression by Flow Cytometry

Pterygia fibroblasts were cultured with recombinant IL-4 (PeproTech, Rocky Hill, NJ) at the selected concentration for 48 hours. To inhibit MAP kinase activity, a highly selective inhibitor of MAP kinase/ERK kinase1 (MEK1), PD98059 (10 μM; New England Biolabs, Beverly, MA), was added to the media. Then the serum-starved fibroblasts were collected by enzyme treatment (Accutase; Innovative Cell Technologies) and incubated for 20 minutes at 37°C in a tube rotator. The fibroblasts were stained by incubation with antiperiostin antibody (1 μg/mL) or control IgG in 0.1% BSA/PBS for 30 minutes at 4°C. After washing, the cells were incubated with Alexa Fluor 488-antirabbit IgG (Molecular Probes, Inc.) for 20 minutes at 4°C. The expression of periostin on the surfaces of the fibroblasts was analyzed (FACSCalibur; Becton-Dickinson, San Jose, CA).

Statistical Analysis

Data are presented as the mean ± SEM. Statistical analyses were performed by unpaired Student's *t*-tests (two tailed) or ANOVA analysis.

Results

Construction of Network Model of Pterygia Recurrence

To understand the global interactions of the pterygia-related genes in terms of their function and regulation, we applied network analysis on the previously determined pterygia transcriptome.[2] We hypothesized this would allow us to determine pterygia recurrence-related biological phenomena in a simplifier form. To construct the network model, differentially induced or suppressed genes in the primary and recurrent pterygia cases were extracted from the whole genome. We focused on a gene set consisting of 184 genes that had a twofold change and that had been shown to contain valid transcriptional information to generate an efficient support vector machine classifier.[2]

When this set of genes was analyzed (Ingenuity Pathway Knowledge Base of known signaling networks; Ingenuity Systems), four major biological networks with high significance scores ($P < 10^{-17}$) were successfully generated (Table 1). Of these, periostin was placed in one of the major networks (network 4), which was annotated as cell cycle, connective tissue development and function, and cell morphology.

The most significant network (network 1) was annotated as cell-to-cell signaling and interaction, hematologic system development and function, and cell cycling. Interestingly, this network predicted vascular endothelial growth factor as the most linked gene, suggesting a role of network 1 in neovascularization processes. Another major network was network 2, which was annotated to function as immune response, cell-to-cell signaling and interaction, and hematologic system development and function and predicted IL-4 as the most linked gene. Another SVM classifier, TIMP-2, was listed in network 3, together with membrane metalloproteinase 7 (MMP7). Top function of the network 3 was annotated as cell death, immunologic diseases, and DNA replication/recombination/repair. Of the previously reported prognosis determinant candidate genes, PSPHL was not found in the generated networks.

TABLE 1. Transcriptional Network of Pterygia Recurrence

Network	Focus Genes	Predicted Genes	Score (−log [*P*])	Functions
1	*ACVR1B, ADRB2, AKAP5, AKAP11, ATP1B1, BTK, CA2, CD97, CHRM1, CYP3A5, DMTF1, GABRG3, GRK5, GRP, MMP1, NPAT, PPBP, THPO*	*CDKN3, CDKN1A, CKLFSF3, CXCL12, DLG4, E2F1, F2, GABRB3, GABRD, IL6, KIF2C, MAPK1, Prlpe, SMTN, SRC, ST5,* ***VEGF***	30	Cell-to-cell signaling and interaction, hematologic system development and function, cell cycle
2	*ACP5, CD1E, CD79B, CR2, IGHM, MS4A1, NCLN, PKNOX1, PLAC8, POU2F2, SATB1, TK2, USP33*	*ALDH1A2, ARG2, CCL24, CCL26, CD1B, CD1C, CEBPB, CLEC7A, CTLA2A, CYSLTR1,* ***IL4****, IL13, INSR, ISG20, LTA4H, MAOA, Retnla, SPRR2B, STAT4, SYNGR2, TFEC, Trim30*	19	Immune response, cell-to-cell signaling and interaction, hematologic system development and function
3	*AP1S1, APOC2, ARHGEF7, DNASE1L3, EHD1, EIF4F1, GSTM1, HIST1H1C, MMP7, SNAP29, TFAM,* ***TIMP2****, TLE4*	*AP1B1, AP1M1, ARL6IP, CIDEC, COL14A1, H2AFZ, HIPK1, HMGN2, KRT15, MT1L, MYC, MYO9B, PDRG1, PLF2, PRKRIR, SLK, TAGLN2, TMSB4x,* ***TNF****, TP53, UBE2S*	19	Cell death, immunologic diseases, DNA replication, recombination, and repair
4	*BF, CEACAM7, DDX11, GDF2, GRIP1, LRMP, PIK3R1,* ***POSTN****, RAB27A, RNASEL, SWAP70, TRPC7*	*ABCG2, ANXA3, C12orf8, CSPG3, EGF, ESR1, FNTA, FSTL1, GJB2, HBP1,* ***HRAS****, HSPB8, Ins1, MYOD1, PFKFB1, PFKM, PPIB, RB1, RPS6KB2, SH2D3A, SYT3, TOM1L1, TRPC6*	17	Cell cycle, connective tissue development and function, cell morphology

Focus genes denote input genes assigned to the calculated networks.
Predicted genes are genes predicted for involvement in the calculated networks.
The most significant gene in the network was underlined.
Significant support vector machine classifiers periostin (POSTN) and TIMP-2 are shown in boldface italic.

Increased Expression of IL-4 in Recurrent Pterygia

Of all the genes either assigned or predicted in the networks, periostin was the SVM classifier of recurrence with the highest accuracy.[2] Periostin has recently been implicated as an adhesion molecule or a tissue remodeling mediator in Th2-type cytokine-mediated diseases,[5] though its roles on the ocular surface remains unexplored. A representative Th2-type cytokine, IL-4, which was predicted in the calculated network 2, is known to induce adhesion molecules or tissue matrix modulators in colon carcinoma cells.[6] Therefore, we hypothesized that IL-4 may contribute to the recurrence process by the induction of gene(s) in the observed networks.

Initially, we used real-time PCR to determine whether the mRNA of IL-4 was transcriptionally induced in pterygia tissues. Analysis of all pterygia cases showed significant induction of IL-4 compared with normal controls (pterygia tissue, 23.5 ± 9.3 relative copies; normal conjunctiva, 0.7 ± 0.5 relative copies/GAPDH; $P < 0.05$). Because tissue remodeling is a critical phenomenon in pterygia recurrence, we next examined whether IL-4 may indeed be induced after recurrence. In recurrence cases, the IL-4 mRNA levels were made worse than the primary cases (Fig. 1). In network 2, another Th2 type cytokine, IL-13, was detected. Therefore, we also examined the IL-13 mRNA levels. In contrast to IL-4, IL-13 was reduced in recurrent cases though the reduction was not statistically significant (primary pterygia, 2.3 ± 2.1 relative copies; recurrent pterygia, 0.07 ± 0.06 relative copies/GAPDH), further supporting an important role of IL-4 in network 2.

Immunohistochemical analysis was performed to confirm that IL-4 was translated in pterygia tissues. Consistent with the transcriptional analysis, IL-4 was prominently expressed in the recurrent tissue and localized mainly in the perivascular tissues and endothelial cells in the stroma of the subconjunctiva (Fig. 1B). Inflammatory cells, including macrophages or lymphocytes, also stained positive for IL-4 and were found focally in the pterygia epithelia. In primary cases, IL-4 was barely detected.

Induction of Periostin by IL-4

To determine the roles played by IL-4 in the constructed networks, we tested whether IL-4 could induce the recurrence classifier, periostin, using pterygia-derived fibroblast cells. Recombinant IL-4-stimulated fibroblasts were examined for periostin mRNA using real-time PCR. Our results showed that IL-4 induced periostin in a dose-dependent manner (Fig. 2A).

For the IL-4-activated genes, ERK1/2-mediated MAP kinase cascade is generally used.[7] To examine an involvement of the ERK1/2 pathway in the transcriptional activation of periostin, IL-4-stimulated-fibroblasts were treated with PD98059, a MEK1 inhibitor. PD98059 significantly inhibited the transcriptional activation of periostin by IL-4 (at 100 pg/mL and 1 ng/mL; $P < 0.05$), indicating an involvement of the MEK1/ERK1 pathway in periostin induction.

We next examined whether the transcriptional activation of periostin may actually translate into periostin expression. Flow cytometric analysis confirmed the expression of periostin by IL-4 (Fig. 2B) compared with control-treated fibroblasts (Fig. 2C). Consistent with the transcriptional outcome, PD98059 treatment inhibited periostin expression (Fig. 2D).

Pterygia Fibroblast Adhesion Mediated by Periostin

Finally, to understand the role of periostin in pterygia recurrence, we examined the functional role of periostin using pterygia-derived fibroblasts. Because pterygial tissues express large amounts of fibronectin, one of the cell matrix ligands of periostin, we tested whether periostin might promote fibronectin-mediated cell adhesion using a cell adhesion assay. Our results showed that fibronectin significantly promoted fibroblast adhesion in a dose-dependent manner (Fig. 3). When fibroblasts were treated with antiperiostin, fibronectin-mediat-

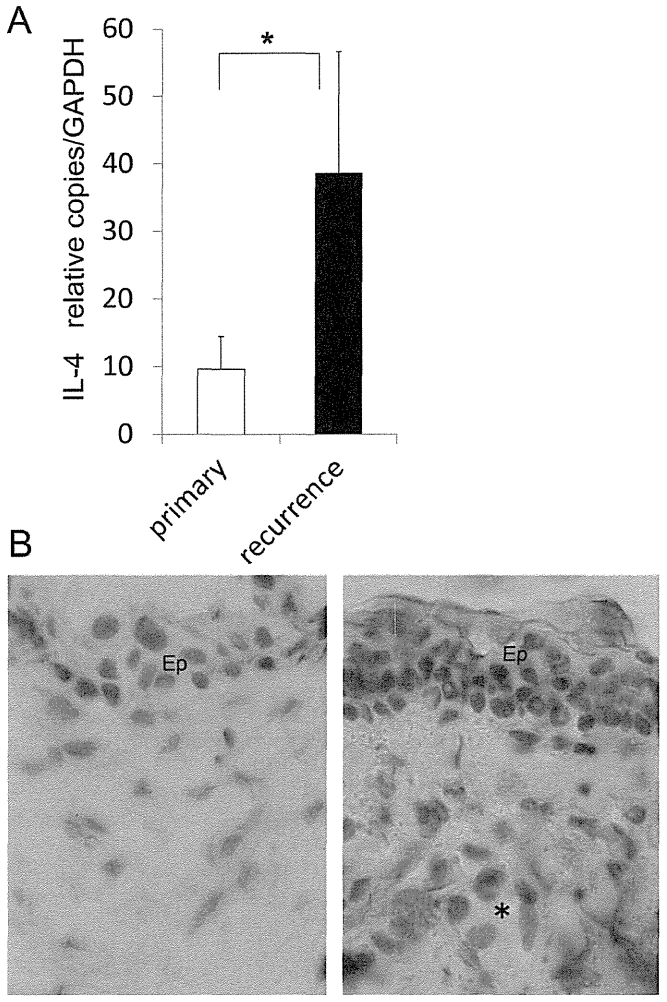

FIGURE 1. Differential expression of IL-4 in primary and recurrent pterygia tissues. (**A**) Recurrent tissues shows significantly more periostin transcript ($P < 0.05$; $n = 11$ eyes for primary tissue; $n = 10$ eyes for recurrent tissue). (**B**) Localization of IL-4 in primary and recurrent pterygia by immunohistochemistry. Upregulated IL-4 expression (*brown*) in epithelium and perivascular tissues of recurrent pterygia (*right*) compared with primary pterygia (*left*). *Asterisks*: inflammatory cells stained positive. Ep, conjunctival epithelium. Original magnification, ×1000.

ed-fibroblast adhesion was significantly inhibited. Thus, periostin was shown to mediate fibroblast adhesion in a fibronectin-rich environment, including pterygia tissue. This critical function of periostin in the pathogenesis of pterygia may promote recurrence.

DISCUSSION

In pterygial tissue, extracellular matrix protein and metalloproteinases (MMPs), including collagen types III and IV, laminin, fibronectin, and MMPs 8, 9, and 13, are abundantly expressed.[8] During the recurrence process, the deposition of such ECM proteins continues and is accompanied by tissue-remodeling processes. These changes eventually lead to marked subepithelial fibrosis.

The results of this study demonstrated a new pathway, leading to pterygia recurrence, that involves IL-4 and periostin. Using knowledge-based bioinformatics, we identified an IL-4 network of immune responses and cell-to-cell signaling, presumably serving as a tissue fibrotic factor in pterygia pathogenesis. For example, in Th2-type diseases, including bronchial asthma, subepithelial fibrosis is a cardinal feature. IL-4 or IL-13 plays an important pivotal role in inducing ECM deposition and subepithelial fibrosis and in exacerbating airway hyperresponsiveness, eosinophil infiltration, and mast cell activation.[5,9-12] However, we observed IL-13 transcripts were greatly reduced, though the reduction was not statistically significant. Because IL-13 is known to compete for IL-4 binding,[13] this may potentiate IL-4 binding. An infiltration of mast cells has been recognized in pterygia tissue; however, a reasonable explanation for the infiltration has not been presented.[14-16] Our findings have revealed a previously unrecognized, but presumably crucial, pathway for pterygia fibrosis.

A recent comprehensive analyses of pterygia transcriptome identified fibronectin as the top induced gene in the genome, followed by other ECM-related genes (e.g., collagen type III and versican).[17] However, IL-4 induction has been unnoticed and hidden in our transcriptome and in others, probably because of its relatively low constitutive levels. Successful identification by network model prediction provided us with an important perspective in pterygia pathogenesis.

From an epidemiologic standpoint, exposure to ultraviolet light (UV) is one of most important factors for the development of pterygia. Indeed, UV exposure induces IL-4 expression in

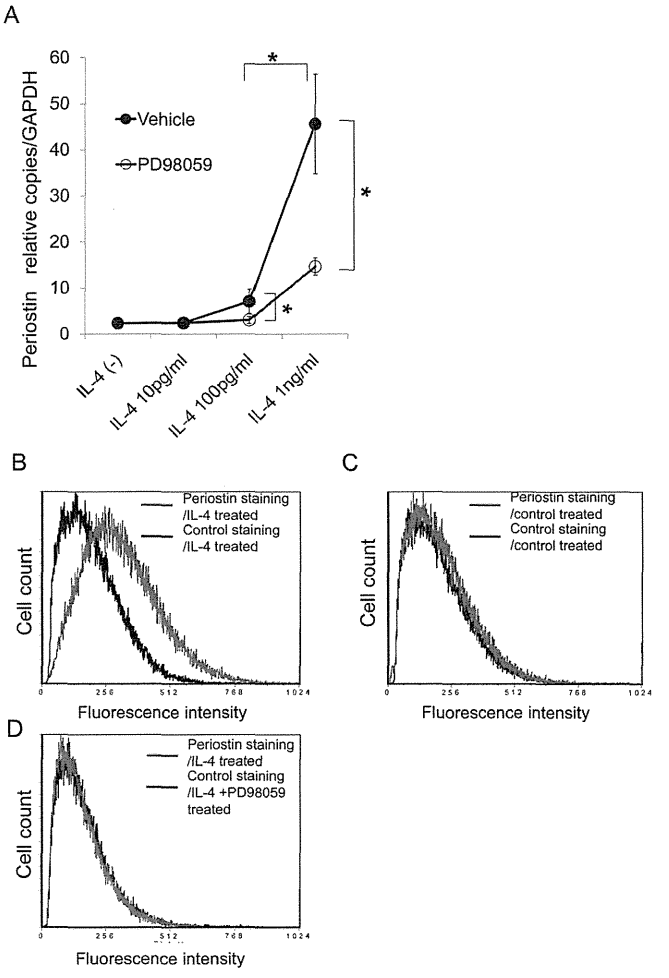

FIGURE 2. Periostin induction of pterygia fibroblast by IL-4. (**A**) IL-4 treatment induced periostin mRNA in a dose-dependent manner at a range of 0 to 1 ng/mL IL-4. Treatment with MEK 1 inhibitor PD98059 (10 μM) significantly suppressed IL-4 induction. *$P < 0.05$; $n = 3$. (**B–D**) Periostin protein expression by IL-4 was examined by flow cytometric analysis. Periostin was induced on pterygia fibroblasts by IL-4 (1 ng/mL) (**B**). No detectable expression of periostin was observed on nonstimulated fibroblasts (**C**). PD98059 (10 μM) inhibited the expression of periostin (**D**). Data are representative of repeated experiments.

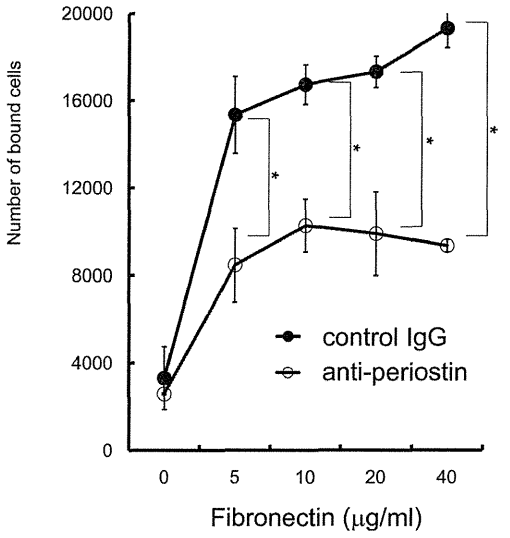

FIGURE 3. Requirement of periostin for fibronectin-mediated adhesion of pterygia fibroblast. Adhesion assay was used to examine the adhesive property of fibroblast to fibronectin-coated wells. Pterygia fibroblasts show fibronectin-dose dependent adhesion. Antiperiostin treatment significantly inhibited fibronectin-mediated adhesion. $^*P < 0.05$; $n = 3$. Data are representative of repeated experiments.

psoriatic tissue and T lymphocytes.[18] Another possible explanation for the differential expression of IL-4 is a possible epigenetic modification of the IL-4 locus by DNA methylation and chromatin remodeling.[19]

Our data suggest that the IL-4-induced periostin may play a critical role in pterygia recurrence. Periostin is an extracellular protein secreted by fibroblasts after injury. The FAS1 domain of periostin interacts with $\alpha_v\beta_3$ and $\alpha_v\beta_5$ integrins and stimulates a fibronectin-dependent motility of epithelial cells.[20,21]

Recently, periostin has been gaining considerable interest in the process of cardiac remodeling or heart failure.[22–24] Periostin associates with critical ECM regulators such as TGF-β, tenascin, and fibronectin and is a critical regulator of fibrosis by altering the deposition and attachment of collagen.[25] Because fibronectin was listed as the top induced gene in the pterygia transcriptome,[17] the IL-4-mediated periostin may constitute a significant component in the pathogenesis of pterygia. Moreover, IL-4 is known to stimulate fibroblasts to induce another recurrence classifier focus gene in network 3, *TIMP2*,[7] which would further promote tissue remodeling.

To summarize, our results have identified new pathologic components in conjunctival fibrosis in pterygia recurrence. Expression of periostin after environmental perturbations, including IL-4 induction, can alter normal physiological interactions between fibroblasts and ECM protein, leading to fibrosis and scar formation. Thus, regulating IL-4/periostin induction may control the recurrence of pterygia.

References

1. Di Girolamo N, Chui J, Coroneo MT, Wakefield D. Pathogenesis of pterygia: role of cytokines, growth factors, and matrix metalloproteinases. *Prog Retin Eye Res.* 2004;23:195–228.
2. Kuo CH, Miyazaki D, Nawata N, et al. Prognosis-determinant candidate genes identified by whole genome scanning in eyes with pterygia. *Invest Ophthalmol Vis Sci.* 2007;48:3566–3575.
3. Ganter B, Giroux CN. Emerging applications of network and pathway analysis in drug discovery and development. *Curr Opin Drug Discov Dev.* 2008;11:86–94.
4. Neidhart M, Zaucke F, von Knoch R, et al. Galectin-3 is induced in rheumatoid arthritis synovial fibroblasts after adhesion to cartilage oligomeric matrix protein. *Ann Rheum Dis.* 2005;64:419–424.
5. Takayama G, Arima K, Kanaji T, et al. Periostin: a novel component of subepithelial fibrosis of bronchial asthma downstream of IL-4 and IL-13 signals. *J Allergy Clin Immunol.* 2006;118:98–104.
6. Herzberg F, Schoning M, Schirner M, Topp M, Thiel E, Kreuser ED. IL-4 and TNF-alpha induce changes in integrin expression and adhesive properties and decrease the lung-colonizing potential of HT-29 colon carcinoma cells. *Clin Exp Metast.* 1996;14:165–175.
7. Ihn H, Yamane K, Asano Y, Kubo M, Tamaki K. IL-4 up-regulates the expression of tissue inhibitor of metalloproteinase-2 in dermal fibroblasts via the p38 mitogen-activated protein kinase dependent pathway. *J Immunol.* 2002;168:1895–1902.
8. Naib-Majani W, Eltohami I, Wernert N, et al. Distribution of extracellular matrix proteins in pterygia: an immunohistochemical study. *Graefes Arch Clin Exp Ophthalmol.* 2004;242:332–338.
9. Zhu Z, Homer RJ, Wang Z, et al. Pulmonary expression of interleukin-13 causes inflammation, mucus hypersecretion, subepithelial fibrosis, physiologic abnormalities, and eotaxin production. *J Clin Invest.* 1999;103:779–788.
10. Foster PS, Ming Y, Matthei KI, Young IG, Temelkovski J, Kumar RK. Dissociation of inflammatory and epithelial responses in a murine model of chronic asthma. *Lab Invest.* 2000;80:655–662.
11. Kumar RK, Herbert C, Yang M, Koskinen AM, McKenzie AN, Foster PS. Role of interleukin-13 in eosinophil accumulation and airway remodelling in a mouse model of chronic asthma. *Clin Exp Allergy.* 2002;32:1104–1111.
12. Komai M, Tanaka H, Masuda T, et al. Role of Th2 responses in the development of allergen-induced airway remodelling in a murine model of allergic asthma. *Br J Pharmacol.* 2003;138:912–920.
13. Obiri NI, Debinski W, Leonard WJ, Puri RK. Receptor for interleukin 13: interaction with interleukin 4 by a mechanism that does not involve the common gamma chain shared by receptors for interleukins 2, 4, 7, 9, and 15. *J Biol Chem.* 1995;270:8797–8804.
14. Nakagami T, Murakami A, Okisaka S, Ebihara N. Mast cells in pterygium: number and phenotype. *Jpn J Ophthalmol.* 1999;43:75–79.
15. Beden U, Irkec M, Orhan D, Orhan M. The roles of T-lymphocyte subpopulations (CD4 and CD8), intercellular adhesion molecule-1 (ICAM-1), HLA-DR receptor, and mast cells in etiopathogenesis of pterygium. *Ocul Immunol Inflamm.* 2003;11:115–122.
16. Ribatti D, Nico B, Maxia C, et al. Neovascularization and mast cells with tryptase activity increase simultaneously in human pterygium. *J Cell Mol Med.* 2007;11:585–589.
17. John-Aryankalayil M, Dushku N, Jaworski CJ, et al. Microarray and protein analysis of human pterygium. *Mol Vis.* 2006;12:55–64.
18. Piskin G, Koomen CW, Picavet D, Bos JD, Teunissen MB. Ultraviolet-B irradiation decreases IFN-gamma and increases IL-4 expression in psoriatic lesional skin in situ and in cultured dermal T cells derived from these lesions. *Exp Dermatol.* 2003;12:172–180.
19. Ansel KM, Lee DU, Rao A. An epigenetic view of helper T cell differentiation. *Nat Immunol.* 2003;4:616–623.
20. Gillan L, Matei D, Fishman DA, Gerbin CS, Karlan BY, Chang DD. Periostin secreted by epithelial ovarian carcinoma is a ligand for alpha(V)beta(3) and alpha(V)beta(5) integrins and promotes cell motility. *Cancer Res.* 2002;62:5358–5364.
21. Kim JE, Jeong HW, Nam JO, et al. Identification of motifs in the fasciclin domains of the transforming growth factor-beta-induced matrix protein betaig-h3 that interact with the alphavbeta5 integrin. *J Biol Chem.* 2002;277:46159–46165.
22. Katsuragi N, Morishita R, Nakamura N, et al. Periostin as a novel factor responsible for ventricular dilation. *Circulation.* 2004;110:1806–1813.
23. Litvin J, Blagg A, Mu A, et al. Periostin and periostin-like factor in the human heart: possible therapeutic targets. *Cardiovasc Pathol.* 2006;15:24–32.
24. Kuhn B, del Monte F, Hajjar RJ, et al. Periostin induces proliferation of differentiated cardiomyocytes and promotes cardiac repair. *Nat Med.* 2007;13:962–969.
25. Borg TK, Markwald R. Periostin: more than just an adhesion molecule. *Circ Res.* 2007;101:230–231.

Cornea

Induction of IL-6 in Transcriptional Networks in Corneal Epithelial Cells after Herpes Simplex Virus Type 1 Infection

Yuki Terasaka, Dai Miyazaki, Keiko Yakura, Tomoko Haruki, and Yoshitsugu Inoue

Purpose. To determine the transcriptional responses of human corneal epithelial cells (HCECs) after herpes simplex virus type (HSV)-1 infection and to identify the critical inflammatory element(s).

Method. Immortalized HCECs were infected with HSV-1, and the global transcriptional profile determined. Molecular signaling networks were constructed from the HSV-1-induced transcriptomes. The relationships of the identified networks were confirmed by real-time-PCR and ELISA. Contributions of the critical network nodes were further evaluated by protein array analyses as candidates for inflammatory element induction.

Results. HSV-1 infection induced a global transcriptional response, with 412 genes significantly activated or suppressed compared with mock-infected HCECs ($P < 0.05$, 2< or 0.5> threshold). Infection by UV-inactivated HSV-1 did not induce significant transcriptional activity. Network analysis showed that the HSV-1-induced transcriptomes were associated with JUN N-terminal kinase, p38, extracellular signal-regulated kinase, and nuclear factor κ-B signaling pathways. These findings indicate that interleukin (IL)-6 and vascular endothelial growth factor (VEGF) probably serve as critical nodes of signaling events. ELISA and protein array analyses verified the induction of the inflammatory elements by HSV infection. Blocking the induction of IL-6 significantly reduced the expression of 21 cytokines, including CCL7, CCL8, CXCL6, transforming growth factor-β2, platelet-derived growth factor, interferon-γ, IL-2, and VEGF, thus confirming the critical role of IL-6.

Conclusions. HCECs respond to HSV-1 infection by initiating mitogen-activated protein kinase-related transcriptional events, and IL-6 may serve to induce expression of an array of inflammatory mediators. (*Invest Ophthalmol Vis Sci.* 2010;51: 2441-2449) DOI:10.1167/iovs.09-4624

Infection of corneal epithelial cells (CECs) by herpes simplex virus type (HSV)-1 can progress to blindness. The prompt use of anti-HSV-1 medications effectively arrests the initial viral infection and replication; however, the disease can still progress to a vision-threatening stage via a secondary wave of inflammatory responses. These responses are mediated by anti-HSV-1 factors or autoimmune responses induced by molecular mimicry.[1-3] Herpetic stromal keratitis (HSK) is exacerbated by frequent reactivation of latent HSV-1 in the trigeminal ganglia, which can eventually lead to severe corneal opacity that requires corneal transplantation.[4-6]

The CECs are the primary target of HSV infections, and they serve as an innate barrier to deeper invasion before the development of acquired immunity. The CECs respond immediately to HSV exposure by releasing inflammatory mediators that recruit leukocytes, including neutrophils and macrophages. The primary responses are needed to establish T-lymphocyte-based acquired immunity. Thus, understanding how CECs respond to HSV infection is important for understanding how the eye reacts to a viral invasion.

CECs react to HSV-1 infection by expressing proinflammatory cytokines, including interferon (IFN)-β, interleukin (IL)-6, tumor necrosis factor (TNF)-α, and IL-8.[7-9] The expression of IL-6, TNF-α, and IL-8 recruits neutrophils and mononuclear lymphocytes and activates their antiviral activity. This first wave, if uncontrolled, leads to corneal neovascularization, which further exacerbates the inflammatory responses and subsequently reduces vision.[10-12]

HSV-1 infections activate signal transduction, including the nuclear factor κ-B (NF-κB) and mitogen-activated protein kinase (MAPK) cascades.[9,13-15] These signaling events most likely result in the release of inflammatory mediators. However, the cellular inflammatory responses differ, depending on the type of host cells and species. HSV-1 infections alter the transcriptional responses of the host which leads to a global suppression of transcriptional events.[3,16]

Several hypothesis-based transcriptional analyses have been conducted that have provided considerable information. However, a global view of the responses of CECs as natural hosts to HSV-1 infection is lacking. Understanding how epithelial cells respond to HSV-1 in the perspective of the whole genome would help establish more efficacious antiviral therapy and management.

The purpose of this study was to gain insight into the complex intertwined biological events in CECs that follow an HSV-1 infection. A bioinformatics-based network analysis of global transcriptional responses was used along with a pathways database of molecular interactions.[17] Our data describe the critical roles of IL-6 in the HSV-1-induced MAPK cascade-related elements.

Materials and Methods

Cells

A human corneal epithelial cell (HCEC) line was kindly provided by Kaoru Araki-Sasaki[18] (RIKEN BioResource Center, Tsukuba, Japan). The HCECs were propagated to confluence on 6- or 96-well plates in DMEM (Dulbecco's modified Eagle's medium; Invitrogen-Gibco, Grand Island, NY) supplemented with 10% fetal bovine serum and used at passages 4 to 6.

From the Division of Ophthalmology and Visual Science, Faculty of Medicine, Tottori University, Tottori, Japan.

Supported by Grand-in-Aid 20592076 for Scientific Research from the Japanese Ministry of Education, Science, and Culture.

Submitted for publication September 10, 2009; revised October 30 and November 15, 2009; accepted November 29, 2009.

Disclosure: **Y. Terasaka**, None; **D. Miyazaki**, None; **K. Yakura**, None; **T. Haruki**, None; **Y. Inoue**, None

Corresponding author: Dai Miyazaki, Division of Ophthalmology and Visual Science, Tottori University Faculty of Medicine, 36-1 Nishicho, Yonago Tottori 683-8504, Japan; dm@grape.med.tottori-u.ac.jp.

Viruses

Confluent monolayers of Vero cells were infected with HSV-1 (KOS strain; the generous gift of Kozaburo Hayashi, Immunology and Virology Section, Laboratory of Immunology, National Eye Institute, Bethesda, MD) The KOS strain was used, because it expresses VEGF, leading to corneal neovascularization, when inoculated onto the mouse eye.[10] After 1 hour of adsorption, the medium containing the virus was aspirated, and the monolayers were refed with fresh HSV-1-free medium. At maximum cytopathic effect, the medium was discarded, and the cells were frozen, thawed, and sonicated in a small amount of remaining medium. The supernatant, collected after centrifugation at 3000 rpm for 10 minutes, was overlaid onto sucrose density gradient (10%–60% wt/vol) and centrifuged with a swing rotor (SW28; Beckman, Fullerton, CA) for 1 hour at 11,500 rpm. The resultant visible band at a lower part of the gradient containing HSV-1 was washed, with centrifugation at 14,000 rpm for 90 minutes, and resuspended in a small volume of serum-free DMEM. The virus was then aliquoted and stored at −80°C until use. The infectivity of the virus was determined by plaque titration assay, typically reaching up to 1×10^9 PFU/mL.

For HSV-1 infection, the HCECs adsorbed the sucrose-density gradient–purified virus stock for 1 hour and then were refed with fresh medium.

Microarray Procedures

HSV-infected HCECs were transcriptionally analyzed by using the whole human genome microarray (Agilent Technologies, Santa Clara, CA) corresponding to 41,000 human genes and transcripts. Mock-infected, UV-inactivated, HSV-infected HCECs were used as the control. Total RNA was isolated from the HSV-infected HCECs 12 hours post infection (PI) (RNeasy Mini Kit; Qiagen, Hilden, Germany), according to the manufacturer's protocol.

Cyanine-3-labeled cRNA was prepared from 0.25 μg of RNA (One-Color Low RNA Input Linear Amplification PLUS kit; Agilent). Fragmented cRNA was hybridized to the whole human genome oligo microarray (G4112F; Agilent) by using a hybridization kit (Gene Expression Hybridization kit, G2545A; Agilent) and was scanned with a microarray scanner (G2565BA; Agilent). The acquired data were bioinformatically analyzed (GeneSpring GX 10; Agilent), and ANOVA was used to extract the genes that were differentially induced or suppressed after HSV infection.

Pathways Analysis

The set of extracted genes was analyzed for transcriptional networks of molecular events (Ingenuity Pathways Analysis 7.0, IPA; Ingenuity Systems, Redwood, CA, computer program based on the Ingenuity Pathways Knowledge Base). The resulting networks were evaluated by the significance scores, which were expressed as the negative logarithm of the probability. The obtained score indicates the likelihood that the assembly of a set of focus genes in a network can be explained by chance alone.

Real-Time RT-PCR

Total RNA was isolated from the HSV-infected HCECs and reverse transcribed (QuantiTect Reverse Transcription Kit; Qiagen). The cDNAs were amplified and quantified on a thermocycler (LightCycler; Roche Applied Science, Mannheim, Germany, with the QuantiTect SYBR Green PCR kit; Qiagen).

The sequences of the real-time PCR primer pairs were: VEGF: forward 5′-GCAGCTTGAGTTAAACGAACG-3′, reverse 5′-GGTTCCCGAAACCCTGAG-3′; IL-6: forward 5′-GATGAGTACAAAAGTCCTGATCCA-3′, reverse 5′-CTGCAGCCACTGGTTCTGT-3′; IFN-α1: forward 5′-GGAGTTTGATGGCAACCAGT-3′, reverse 5′-CTCTCCTCCTGCATCACACA-3′; and glyceraldehyde-3-phosphate dehydrogenase (GAPDH): forward 5′-AGCCACATCGCTCAGACAC-3′, reverse 5′-GCCCAATACGACCAAATCC-3′.

Equal loading and amplification were ensured by normalizing all products to the GAPDH transcript as an internal control.

ELISA

The levels of secreted IL-6 and VEGF was determined by assaying supernatants collected from HSV-infected HCECs with commercial ELISA kits (Peprotech, Rocky Hill, NJ). Anti-human IL-6 antibody (clone: MQ2-13A5, Biolegend, San Diego, CA) was used to neutralize IL-6 activity.

Cytokine Array Analysis

For inflammatory cytokine profiling after HSV infection, supernatants were collected from HCECs 12 hours PI and assayed with a protein array system (Human Cytokine Antibody Array; RayBiotech, Norcross, GA). This system determines the level of expression of 80 cytokines. The intensity of the chemiluminescence signals was digitized (LAS-1000plus; Fujifilm, Tokyo, Japan, and MultiGauge software ver.2.0; Fujifilm) and normalized by using the positive control signals in each membrane.

Statistical Analyses

Data are expressed as the mean ± SEM. Statistical analyses were performed by using *t*-tests or ANOVA, as appropriate.

Results

Microarray Analysis of HSV-Infected HCECs

To dissect the transcriptional responses of HCECs to HSV-1 infection, we first analyzed the IFN responses of HCECs by using real-time PCR. After HSV-1 infection, the level of IFN-α1 transcript was significantly increased at 12 hours PI—that is, the IFN-α1 expression relative to GAPDH was 2.7 ± 0.2 (relative copies) at multiplicity of infection (MOI) 1 of HSV-1 and 1.6 ± 0.1 (relative copies) for mock infection ($P < 0.01$). The level was increased at 24 hours PI to 31.3 ± 7.7 (relative copies) IFN-α1/GAPDH at MOI 1 of HSV-1 and 2.9 ± 0.5 (relative copies) for mock infection ($P < 0.05$). At 6 hours PI, no appreciable increase was observed. These findings indicated that the response to the HSV infection occurred at 12 hours PI and increased thereafter.

Next, we conducted a global transcriptional profiling of HSV-infected HCECs by microarray analysis of HSV-infected, mock-infected, and UV-inactivated HSV-infected HCECs at the end of the inflammatory responses. We identified 13,594 genes that were differentially expressed in HSV-infected cells at 12 hours PI (ANOVA; $P < 0.05$). To extract sets of virus-responsive genes, we then applied ANOVA with the threshold of twofold expression changes. This analysis resulted in the detection of 412 genes with significantly different expression in the three groups ($P < 0.05$); 365 genes were upregulated and 47 were downregulated in the HSV-infected HCECs.

These genes were analyzed for hierarchical clustering. The resulting dendrograms showed that most of the genes were upregulated after HSV infection (Fig. 1). HSV-infected HCECs showed a distinctive expression profile, in contrast with barely discernible profiles in mock- or UV-inactivated HSV-treated HCECs. The upregulated genes at the highest ratio were *RAS*, dexamethasone-induced 1 (*RASD1*), family with sequence similarity 90, member A10 (*FAM90A10*), *LOC387763*, *FLJ00049*, v-maf musculoaponeurotic fibrosarcoma oncogene homologue A (*MAFA*), and growth arrest and DNA-damage-inducible, gamma (*GADD45G*), among the annotated network-eligible genes (Supplementary Table S1, http://www.iovs.org/cgi/content/full/51/5/2441/DC1). Of these, *RASD1*, *MAFA*, and *GADD45G* generally represent involvement of stress-induced pathways, including the MAPK cascade.

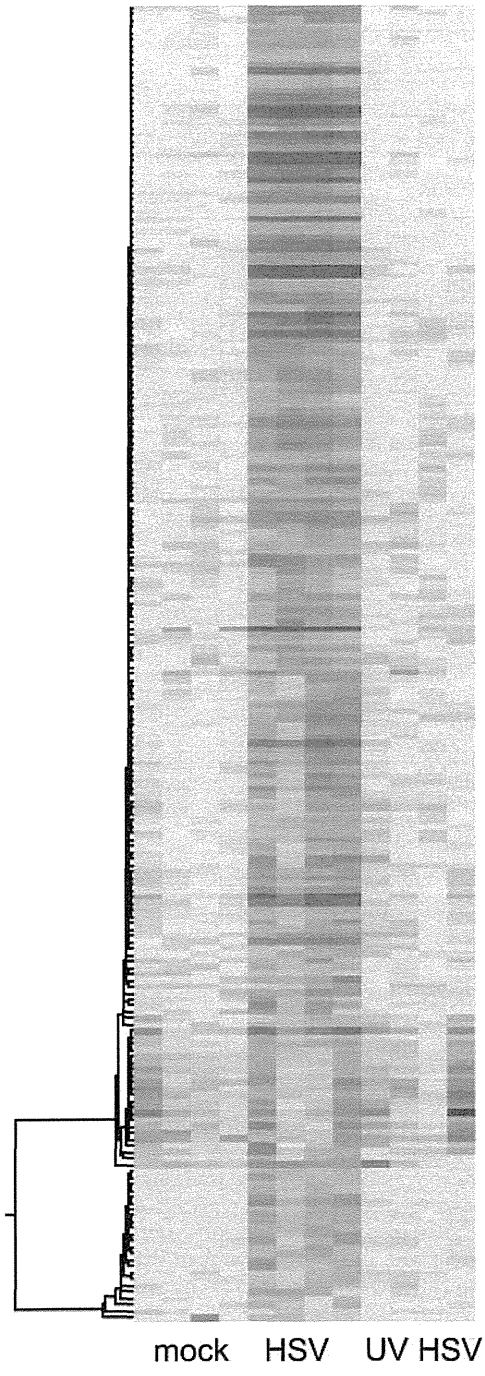

FIGURE 1. Clustering analysis of HSV-1 infection-induced transcriptome in an HCEC line. Four hundred twelve differentially expressed genes (ANOVA; $P < 0.05$, 2< or 0.5> threshold, 12 hours PI) were analyzed by using hierarchical clustering. Gene direction analysis showed that HSV-1 KOS strain infection, but not UV-inactivated HSV-1 infection, induced transcriptional alteration at 12 hours PI. The expression levels are color coded (*red*, activated; *green*, suppressed). n = 4/group.

The downregulated genes at the highest ratio were short-chain dehydrogenase/reductase family 42E, member 1 (HSPC105), zinc finger-BED-type containing 2 (*ZBED2*), and kelch-like 24 (*KLHL24*). In the HCECs exposed to UV-inactivated HSV, the transcriptional profile was almost identical with mock-infected HCECs, with the exception of 11 genes that were differentially expressed.

Network Analysis of Altered Genes in HSV-Infected HCECs

To obtain a global view of the HSV infection-induced phenomenon and determine therapeutic candidate inflammatory mediator gene(s) for herpetic keratitis, we analyzed the 412 extracted genes for signaling interactions by using a systematic biological approach. We successfully generated five major biological networks with high significance scores ($P < 10^{-26}$) using a database of known signaling networks (Ingenuity Pathways Knowledge Base; Ingenuity Systems; Table 1).

Network 1 was the most significant network of focus genes: *FOS*, *JUN*, *BCL2*-associated X protein (*BAX*), and zinc finger protein 36 (*ZFP36*). Network 1 included genes annotated as cell cycle, cell death, and neurologic diseases. Network 2 contained those annotated as cancer, cellular growth and proliferation, and respiratory diseases, and were represented by the focus genes *GADD45* and dual specificity phosphatase 1 (*DUSP1*), which are related to stressful *GADD*. These were classified as MAPK/extracellular signal-regulated kinase (ERK) cascade by network analysis. In this network, the upstream inflammatory mediators *PDGF*, *CXCL1*, and insulin-like growth factor (IGF)-2 were also upregulated.

Network 3 contained genes annotated as skeletal and muscular system development and function, cancer, and cell-to-cell signaling and interaction, and involved the upregulation of the arachidonic acid cascade mediator, phospholipase A2 (*PLA2*), and a transcriptional activator downstream of Ca^{2+} or cyclic AMP (cAMP) responsive element binding protein (CREBBP). Network 4 included genes annotated as connective tissue disorders, genetic disorders, and immunologic diseases, with upregulation of the inflammatory cytokines CCL5 and CXCL2, in addition to IL-6 induction.

Network 5 genes were annotated as cell cycle and skeletal and muscular system development and function and cancer, characterized by the induction of VEGF, endothelin 1 (EDN1), connective tissue growth factor (CTGF), heparin binding EGF-like growth factor (HBEGF), and cyclooxygenase (PTGS2).

Of the five signaling networks, we identified a proinflammatory focus gene, *IL-6* in network 4, as the most significant canonical inflammatory mediator in terms of the number of interactions in the signaling networks. Because IL-6 generally serves as a critical inflammatory coordinator downstream of the pattern recognition receptors, which serve as a first line of defense against pathogens, we then analyzed the HSV-induced transcriptional networks in relation to *IL-6*.

To understand the transcriptional roles of IL-6 in the constructed networks, we merged networks 1 to 5 to give an overview (Fig. 2). Because IL-6 was centrally positioned in this view of the networks, we next explored whether it orchestrates the induction of the inflammatory mediators. In the merged network, we observed VEGF as a crucial node. VEGF has gained the interest of researchers for its involvement in corneal neovascularization at the later stage of HSK, and the neovascularization is typically followed by the establishment of epithelial lesions.[10] Therefore, we hypothesized that there is a direct relationship of IL-6 and VEGF in the epithelial transcriptome.

Inductive Effect of IL-6 on VEGF in HSV-Infected HCECs

We first determined whether IL-6 is expressed in HSV-infected HCECs by using real-time PCR. IL-6 was detected as early as 3 hours PI, and the level peaked at 12 hours (Fig. 3A). To confirm that IL-6 is translated, we used ELISA to assay the supernatants collected from the HSV-infected HCECs at 12 hours. Secreted IL-6 was elevated in HSV-infected HCECs in a dose-dependent manner, and the level increased until 24 hours PI (Fig. 3B). At

TABLE 1. Transcriptional Networks of HSV-Infected Corneal Epithelial Cells

Network	Focus Genes	Predicted Genes	Score = −log (*P*)	Functions
1	*ARF1, BAX, BCL2L11,* Calpain, *CAPN1, CCNG2, CD274, CDKN1C, CRABP1, EEF1D, FOS, GALNT11, GRASP, ID2, ING1, JUN, JUNB, MGEA5, MYCN, NFYA, OSBP2, PDCD1, PDCD4, SPRY4, VIM, ZFP36*	Caspase, Cyclin A, Cytochrome C, *FGF,* Hexokinase, Proteasome, Rb, Smad, Ubiquitin	46	Cell cycle, cell death, neurological disease
2	*ADM, CXCL1, DUSP1, DUSP4, DUSP6, IER2, GADD45, GADD45A, GADD45B, GADD45G, IGF2, JUN/JUNB/JUND, KLF2, MKP1/2/3/4, MXD1, THBD,* Thyroid hormone receptor, *PDGF-AB, PDGF-AA, PDGFA, PHLDA1, PNRC1, RASD1, VAV3*	ERK, GC-GCR dimer, JINK1I2, Laminin, N-cor, Notch, *Pak, Rar, Rxr, SWI-SNF,* VitaminD3-*VDR-RXR*	29	Cancer, cellular growth, and proliferation, respiratory disease
3	ATAD4, BMF, Cbp/p300, CBX4, CREBBP, DLX2, EPHA4, *GABARAPL1, MED26, MLL, MSX1, MYLK2, NOC2L, OSGIN1, PDXK, PLA2, PLA2G6, SENP3, WISP2*	Actin, Calmodulin, *Ck2, ERK1I2, FSH,* Histone h3, Histone h4, Hsp70, *MAPK, Pka, Pld, PP2A, RGS2,* RNA polymerase II, *STAT5a/b,* Tubulin	29	Skeletal and muscular system development and function, cancer, cell-to-cell signaling and interaction
4	*CARD9, CCL5, CDKN2C, CXCL2,* Cyclooxygenase, *DUSP2, IER3, IFN-b, IL6, IRF9, MUC2, ND2, PIM2* (includes EG:11040), *RGS16, RSAD2, SELPLG, SOCS1, TLR, TLR1, TNFAIP3*	*ALP,* Hsp27, *IFN-a, IFN-g, IgG, IL1, IL12, IRF, JAK, LDL,* MHC Class I, *NF-κB, STAT, TGF-β*	27	Connective tissue disorders, genetic disorder, immunological disease
5	*CTGF, CXCR4, DLL1, DUSP8, EDN1, EREG, ERN1* (includes EG:2081), *MBTPS1, MYH3,* Myosin, *OASL, PTGS2, SNAI1, SP100, SYNJ1, THRA, VEGF*	*ADCY,* Calcineurin protein(s), G-protein-β, *HBEGF, HCG, Ige, IKK, JNK, Mek, MMP, Nos, p38 MAPK, p70 S6k, Pkc(s), PLC, PLC-g,* Tyrosine kinase	26	Cell cycle, cancer, skeletal and muscular system development and function

Focus genes denote assigned input genes to the calculated networks. Predicted genes are genes predicted for involvement in the calculated networks.

12 hours PI, VEGF secretion was also significantly elevated in the HSV-infected HCECs (Fig. 4A). UV-inactivated HSV did not stimulate IL-6 and VEGF secretion (data not shown).

To examine the role played by IL-6, we evaluated HSV-infected HCECs for VEGF induction after blocking IL-6 with anti-IL-6 antibody (Fig. 4A) and found that a significantly lower level of VEGF was secreted from the infected HCECs. To determine whether the reduced VEGF level was due to a blockage of virus replication, we used real-time PCR[19] and a plaque assay to quantify the HSV-1 genome. Replication of the HSV-1 genome was not significantly affected by IL-6 blockade (cells control treated at MOI 0.1 yielded $9.2 \pm 0.9 \times 10^3$ copies/μL and anti-IL-6-treated at MOI 0.1 yielded $1.0 \pm 0.2 \times 10^4$ copies/μL, $P > 0.05$). A plaque assay showed that the replication of the HSV-1 genome was not affected by the anti-IL-6 antibody (Fig. 4B). Thus, the decreased VEGF secretion induced by the IL-6 blockade appeared not to be the direct effect of altered HSV replication. In addition, when HCECs were exposed to recombinant IL-6 without HSV infection, they did not secrete VEGF (Fig. 4C). This finding indicates that activation of VEGF expression in HCECs requires both IL-6 and HSV-induced factors.

Network Analysis of IL-6 and Related Inflammatory Cytokines in HSV-Infected HCECs

The outcome of these experiments (Figs. 3, 4) and the network analyses (Fig. 2) suggests that IL-6 plays a role in HSV-infected HCECs. In general, IL-6 is one of the major physiological mediators of acute phase reactions and is associated with or activates many inflammatory cytokines. Because IL-6 can orchestrate or modulate the inflammatory milieu of HCECs, we next determined the cytokine species that are dependent on IL-6. HCECs were infected with HSV at MOI 1, allowed 1 hour for adsorption, and then fed control IgG or anti-IL-6 antibody, added to the DMEM. After 12 hours of incubation, the supernatants of HSV-1-infected HCECs were collected and assayed with a cytokine array. After the HSV-1 infection, the release of many inflammatory cytokines, both reported ones and unrecognized ones, was induced. IL-6 was among the top five induced genes after *GRO, CCL7, IL-6, CCL8,* and *IL-8,* in descending order. This result again supports our proposal that *IL-6* plays a critical role in the HSV-induced transcriptome.

When 55 HSV-induced cytokines (normalized relative intensity >1.0) were analyzed for possible IL-6 dependency, we detected a significant reduction of 21 of them after anti-IL-6 treatment, including CCL7, CCL8, CXCL6, TGF-β2, and PDGF in descending order ($P < 0.05$; Fig. 5). Consistent with the data in Figure 4, we confirmed an IL-6 dependence of VEGF.

To summarize the relationship of IL-6 and the IL-6-sensitive mediators, we further applied network analysis to them. When we used the representative network nodes with the significant edges identified in Figure 2, the interactions of IL-6 and the identified IL-6-sensitive cytokines (Fig. 5) were associated with to the MAPK cascade-related elements.

DISCUSSION

We used a bioinformatics-based approach to analyze the response of HCECs to HSV-1 infection. Our results showed that HSV infection affected the expression of numerous genes, and most of the mRNAs were transcriptionally activated. This global transcriptional activation was also observed by Ka-

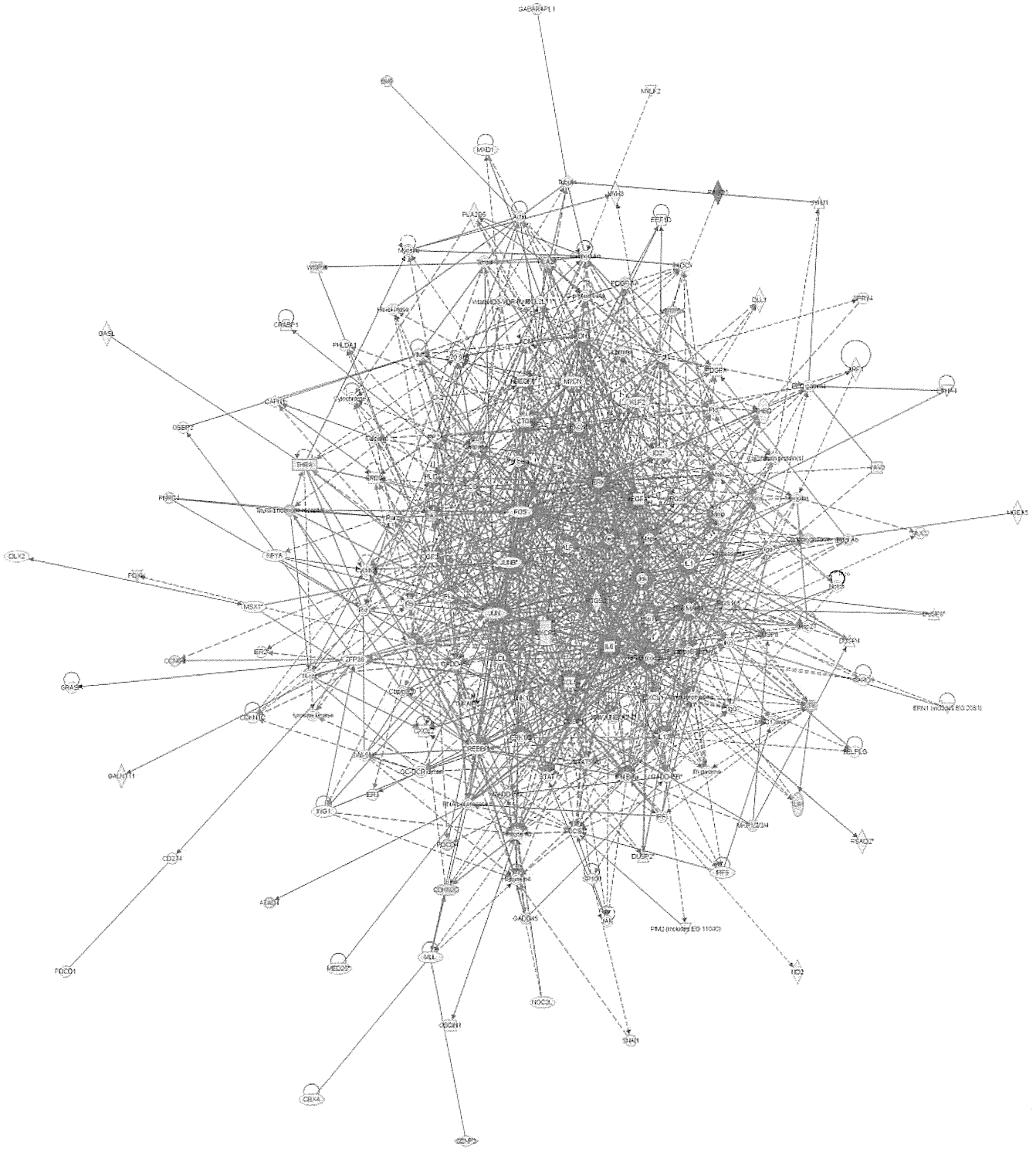

FIGURE 2. Pathway analysis of the biological processes underlying the HSV-1 infection-induced responses of HCECs. Networks 1 to 5 form the merged network. *Red*, activated; *green*, suppressed.

makura et al.,[20] who showed that most of the genes in the transcriptome of the HEp-2 epithelial cells were upregulated at 9 hours PI. Their results and our results are in striking contrast to the results of a microarray analyses of nonepithelial permissive cell lines (embryonic lung cells or HeLa),[21–23] which showed most of the cellular transcripts to be downregulated. These changes are considered to be mediated by transcriptional suppression of the host genes by viral proteins or immediate early genes.

In epithelial cells, including HCECs, our results and those of Kamakura et al.[20] showed a marked transcriptional upregulation, which may be related to or caused by epithelial-specific factors that act as a primary defense system and initiate the expression of an arsenal of proinflammatory mediators.

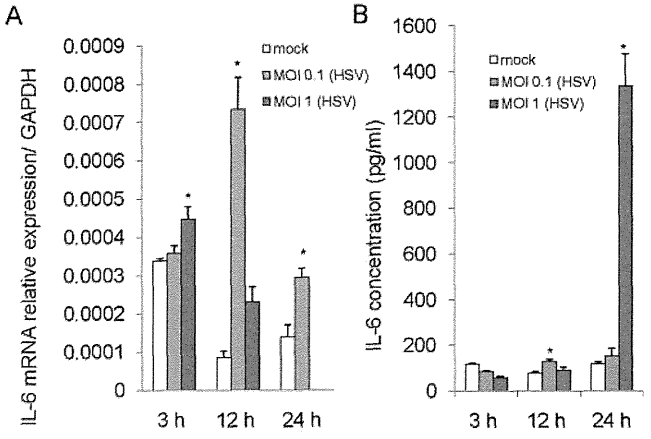

FIGURE 3. Kinetics of IL-6 induction in HCECs after HSV-1 infection. The mRNA of IL-6 is significantly induced at 3 hours PI and peaked at 12 hours PI, as determined by real-time RT-PCR (**A**). The IL-6 level in the infected supernatant was significantly elevated, as determined by ELISA (**B**). $n = 6$; $^*P < 0.05$.

A global view of the HSV-induced host genes by network analysis clearly showed significant involvement of the JNK, p38, ERK, and NF-κB signaling pathways and related elements. Activation of NF-κB and JNK has been shown to be related to

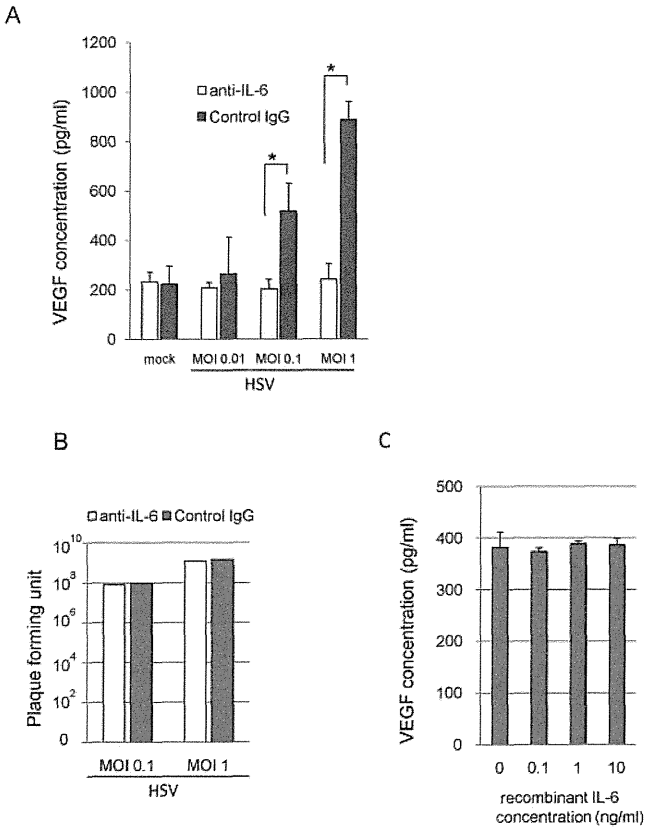

FIGURE 4. Requirement of IL-6 and HSV-1 infection for VEGF induction in the HCECs. HSV-1 infection significantly induced VEGF at 12 hours PI which was suppressed by anti-IL-6 treatment (**A**). The supernatant of HSV-1-infected corneal epithelial cells was assayed for HSV-1 titration. There were no significant differences of virus titers in control IgG and anti-IL-6 treatment (**B**). Stimulation by recombinant IL-6 without HSV-1 infection failed to induce VEGF production by corneal epithelial cells (**C**). $n = 4$; $^*P < 0.01$.

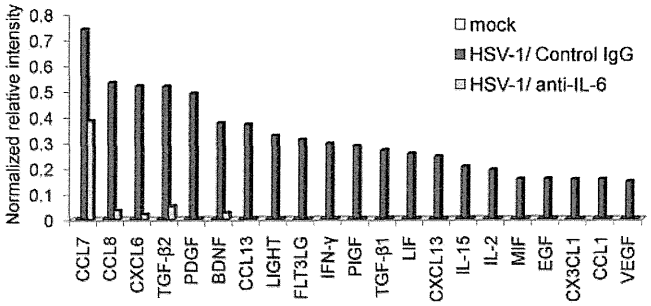

FIGURE 5. IL-6-sensitive induction profile of inflammatory cytokines by HSV-1-infected HCECs. HCECs adsorbed HSV-1 at MOI 1 for 1 hour and were refed with DMEM containing control IgG or anti-IL-6 antibody. After 12 hours of incubation, the supernatant of HSV-1-infected HCECs was assayed with a cytokine array. A panel of the inflammatory cytokines significantly suppressed by IL-6 blockade is shown. n = 4/group; $P < 0.05$.

the induction of inflammatory cytokines including IL-6, IL-8, and TNF-α.[9] In our attempt to understand the molecular relationship of signaling molecules and inflammatory cytokines, network analyses identified IL-6 as the most significant element. Although IL-6 has been noted to be an important inflammatory mediator after HSV infection[24] of epithelial cells, our analyses showed a new role of IL-6 at the whole-genome level. IL-6 is a pleiotropic cytokine and mediates acute phase reaction that influences antigen-specific immune responses.[25,26] IL-6 is an important B-cell differentiation factor as well as a convertor of T cells into cytotoxic T cells or Th17 lineage.[27] Considering the exacerbating role of IL-6 in the inflammatory response, the virulence of an HSV strain may be related to the inducibility of IL-6. For example, the MP strain has been reported to be a more potent inducer of IL-6 than the KOS strain[8] and is able to elicit more aberrant immune responses in the eye. Another important property of IL-6 is its neurotrophic function, which promotes neuronal survival.[28] The promotion of neuronal survival by IL-6 may induce ocular reactivation of latent HSV-1 in the trigeminal ganglion.[29]

In herpetic keratitis, IL-6 has been documented to be a factor that contributes to the massive neutrophil attraction to the corneal stroma.[8,30,31] Also, IL-6 has been reported to be related to corneal neovascularization via VEGF, another cardinal feature of herpetic keratitis.[8,31,32] The induction of VEGF in herpetic keratitis has been thought to be mediated in a paracrine manner by IL-6-producing bystander populations such as noninfected inflammatory cells.[31] However, the corneal epithelium has not been noted as a autocrine source of VEGF.

Our findings on HCECs' participation in an autoamplifying loop after infection provide a new and important perspective on epithelial function as a host defense mechanism. However, this effect has the potential to lead to HSK. Neovascularization is not usually observed in epithelial keratitis, but our findings suggest that the molecular background of HSK has already been set at an earlier stage of epithelial keratitis.

In the HSV-induced network (Fig. 2), IL-6 has been centrally placed in the transcriptional upregulation of CXCL1, FOS, JUNB, HBEGF, GADD45B, inhibitor of DNA binding 2 (ID2), and ZFP36.[33–35] Of these, FOS, JUNB, and GADD45 respond to environmental stresses by activating the MAPK pathways. FOS and JUN are especially critical transcription factors and are involved in numerous canonical pathways, including signaling by MAPK, acute phase responses, and signaling by the chemokines IL-2/IL-6/IL-17/PDGF, stress-activated protein kinase (SAPK)/JNK, TGF-β, nuclear factor of activated T cells, and Toll-like receptor (TLR). FOS and JUN directly regulate the

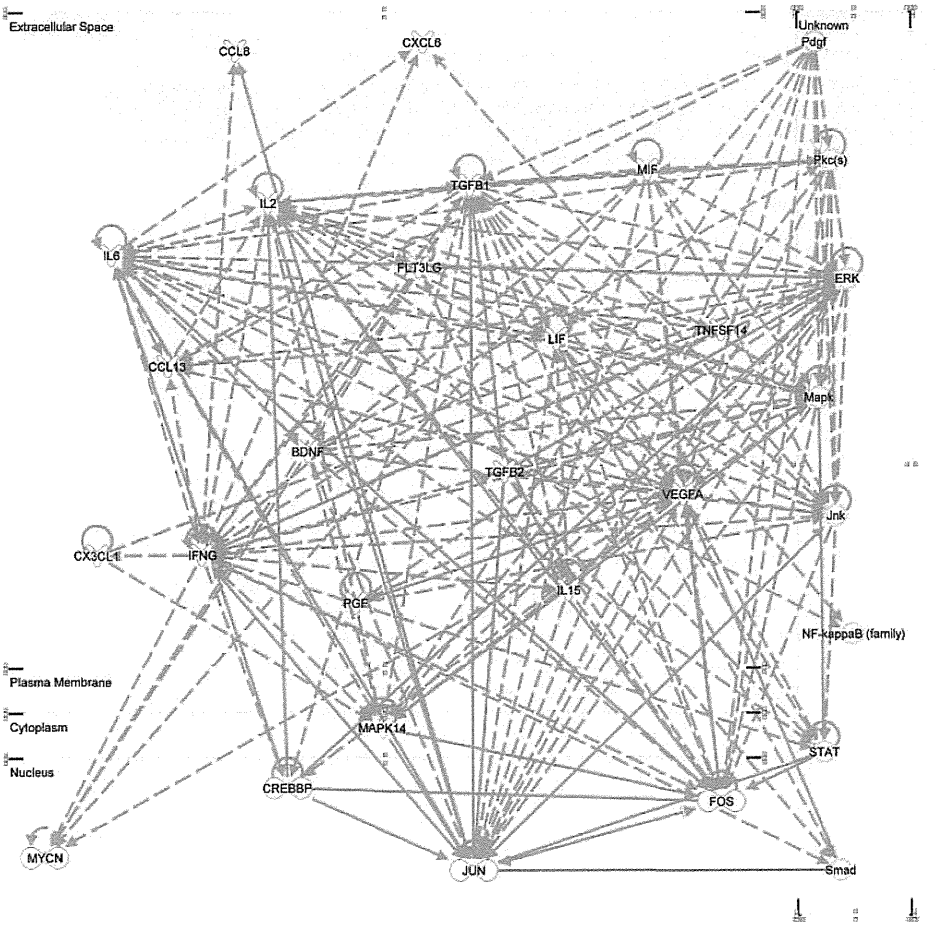

FIGURE 6. Pathway analysis of IL-6-senstive inflammatory cytokine induction and canonical pathways underlying HSV-1-infection.

critical inflammatory mediators IL-6, VEGF, IL-2, IL-8, and cyclooxygenase (Fig. 2).[33,36–42] When we analyzed the cytokine profiling sensitive to the blockade of IL-6, we found numerous previously unrecognized IL-6-sensitive genes, including *TGF-B2*, *PDGF*, *BDNF*, *CCL13*, *LIGHT*, *FLT3LG*, *IFN-G*, *PIGF*, *TGF-B1*, *IL-15*, *MIF*, and *CX3CL1*, together with previously reported genes, including *CXCL6*, *IL-2*, *CCL1*, *LIF*, *VEGF*, and *BDNF*.[8,27,31,43–47] These interactions were associated with IL-6, IL-2, IFN-γ, TGF-β1,. and VEGF (Fig. 6) and appeared to intricately regulate each other by interacting with ERK, MAPK, JNK, FOS, JUN, and MAPK14 (Fig. 6).

The induction of IL-6 is generally dependent on the activation of the NF-κB and p38 pathways.[48] HSV infection stimulates transcriptional activation of the NF-κB, CRE, and activator protein (AP)-1 recognition sites in the *IL-6* gene as early as 1 hour to 2 hours PI[9,48,49] and supports the suggestion that IL-6 induction at the very early stage of infection activates inflammatory mediators. However, the triggering mechanism of IL-6 has not been completely determined.

Keratocytes have been shown to express IL-6 after HSV infection in a TLR3- and TLR9-dependent manner without requiring transcriptionally competent HSV.[8] However, TLR9 stimulation requires very high levels of HSV DNA, far exceeding the concentration used in our study. In HSV-infected macrophages, IL-6 expression was shown to be mediated by RNA-activated protein kinase (PKR), which senses the accumulation of viral double-stranded RNA in the infected cells.[48] PKR-mediated IL-6 expression is independent of virion transacting protein 16 (VP16) or immediate early proteins, including infected cell protein (ICP)-0, -4, and -27, and requires transcriptionally competent HSV. This finding is consistent with our observation of defective transcriptional activation in UV-inactivated HSV at the whole-genome level (Fig. 1). Induction of IL-6 expression in the presence of the HSV-induced transcriptome appears restricted to CECs or keratocytes as host cells.[8,20,50–52] A significant involvement of IL-6, which is characteristic of corneal cells or other host-derived factors, may specifically determine the transcriptional responses dependent on the functionality of the host cells.

Our microarray analysis detected a prominent upregulation of stress-related genes, including *RASD1*, *GADD45G*, and snail homolog 1 (*SNAI1*). In addition, cancer formation–related genes, including *MAFA*, zinc finger protein 296 (*ZNF296*), *IGF-2*, and gastrulation brain homeobox 2 (*GBX2*), among the top activated genes, were upregulated (Supplementary Table S1, http://www.iovs.org/cgi/content/full/51/5/2441/DC1).[20,49,51,53] The expression of the *RASD1* and *GADD45* proteins ZNF296 and IGF-2 are generally observed after HSV infection in microarray analyses depending on the cell type and the strain. In contrast, a strong expression of *MAFA* appears characteristic of CECs. MAFA belongs to the AP-1 transcription factor family, as do JUN and FOS, and is activated by phosphorylation by the p38 MAPK pathway.[54] It has strong cell-transforming/transactivation capabilities and has recently gained interest in oncogenesis.[55]

To summarize, HSV-infection of HCECs induces an inflammatome relating to transcriptional events involving ERK, MAPK, JUNK, and NF-κB and uses IL-6 as a critical element to regulate proinflammatory cytokine induction.

Acknowledgments

The authors thank Duco Hamasaki for editing the article.

References

1. Verjans GM, Remeijer L, Mooy CM, Osterhaus AD. Herpes simplex virus-specific T cells infiltrate the cornea of patients with herpetic stromal keratitis: no evidence for autoreactive T cells. *Invest Ophthalmol Vis Sci.* 2000;41:2607-2612.
2. Deshpande SP, Zheng M, Lee S, Rouse BT. Mechanisms of pathogenesis in herpetic immunoinflammatory ocular lesions. *Vet Mtcrobiol.* 2002;86:17-26.
3. Banerjee K, Biswas PS, Rouse BT. Elucidating the protective and pathologic T cell species in the virus-induced corneal immunoinflammatory condition herpetic stromal keratitis. *J Leukoc Biol.* 2005;77:24-32.
4. Liesegang TJ. Herpes simplex virus epidemiology and ocular importance. *Cornea.* 2001;20:1-13.
5. Branco BC, Gaudio PA, Margolis TP. Epidemiology and molecular analysis of herpes simplex keratitis requiring primary penetrating keratoplasty. *Br J Ophthalmol.* 2004;88:1285-1288.
6. Xie L, Song Z, Zhao J, Shi W, Wang F. Indications for penetrating keratoplasty in north China. *Cornea.* 2007;26:1070-1073.
7. Miyazaki D, Inoue Y, Araki-Sasaki K, Shimomura Y, Tano Y, Hayashi K. Neutrophil chemotaxis induced by corneal epithelial cells after herpes simplex virus type 1 infection. *Curr Eye Res.* 1998; 17:687-693.
8. Hayashi K, Hooper LC, Chin MS, Nagineni CN, Detrick B, Hooks JJ. Herpes simplex virus 1 (HSV-1) DNA and immune complex (HSV-1-human IgG) elicit vigorous interleukin 6 release from infected corneal cells via Toll-like receptors. *J Gen Virol.* 2006;87: 2161-2169.
9. Li H, Zhang J, Kumar A, Zheng M, Atherton SS, Yu FS. Herpes simplex virus 1 infection induces the expression of proinflammatory cytokines, interferons and TLR7 in human corneal epithelial cells. *Immunology.* 2006;117:167-176.
10. Zheng M, Deshpande S, Lee S, Ferrara N, Rouse BT. Contribution of vascular endothelial growth factor in the neovascularization process during the pathogenesis of herpetic stromal keratitis. *J Virol.* 2001;75:9828-9835.
11. Zheng M, Klinman DM, Gierynska M, Rouse BT. DNA containing CpG motifs induces angiogenesis. *Proc Natl Acad Sci U S A.* 2002;99:8944-8949.
12. Kim B, Tang Q, Biswas PS, et al. Inhibition of ocular angiogenesis by siRNA targeting vascular endothelial growth factor pathway genes: therapeutic strategy for herpetic stromal keratitis. *Am J Pathol.* 2004;165:2177-2185.
13. McLean TI, Bachenheimer SL. Activation of cJUN N-terminal kinase by herpes simplex virus type 1 enhances viral replication. *J Virol.* 1999;73:8415-8426.
14. Zachos G, Clements B, Conner J. Herpes simplex virus type 1 infection stimulates p38/c-Jun N-terminal mitogen-activated protein kinase pathways and activates transcription factor AP-1. *J Biol Chem.* 1999;274:5097-5103.
15. Amici C, Belardo G, Rossi A, Santoro MG. Activation of I kappa b kinase by herpes simplex virus type 1: a novel target for antiherpetic therapy. *J Biol Chem.* 2001;276:28759-28766.
16. Koelle DM, Reymond SN, Chen H, et al. Tegument-specific, virus-reactive CD4 T cells localize to the cornea in herpes simplex virus interstitial keratitis in humans. *J Virol.* 2000;74:10930-10938.
17. Kuo CH, Miyazaki D, Yakura K, Araki-Sasaki K, Inoue Y. Role of periostin and interleukin-4 in recurrence of pterygia. *Invest Ophthalmol Vis Sci.* 2010;51(1):139-143.
18. Araki-Sasaki K, Ohashi Y, Sasabe T, et al. An SV40-immortalized human corneal epithelial cell line and its characterization. *Invest Ophthalmol Vis Sci.* 1995;36:614-621.
19. Kakimaru-Hasegawa A, Kuo CH, Komatsu N, Komatsu K, Miyazaki D, Inoue Y. Clinical application of real-time polymerase chain reaction for diagnosis of herpetic diseases of the anterior segment of the eye. *Jpn J Ophthalmol.* 2008;52:24-31.
20. Kamakura M, Nawa A, Ushijima Y, et al. Microarray analysis of transcriptional responses to infection by herpes simplex virus types 1 and 2 and their US3-deficient mutants. *Microbes Infect.* 2008;10:405-413.
21. Khodarev NN, Advani SJ, Gupta N, Roizman B, Weichselbaum RR. Accumulation of specific RNAs encoding transcriptional factors and stress response proteins against a background of severe depletion of cellular RNAs in cells infected with herpes simplex virus 1. *Proc Natl Acad Sci U S A.* 1999;96:12062-12067.
22. Stingley SW, Ramirez JJ, Aguilar SA, et al. Global analysis of herpes simplex virus type 1 transcription using an oligonucleotide-based DNA microarray. *J Virol.* 2000;74:9916-9927.
23. Mossman KL, Macgregor PF, Rozmus JJ, Goryachev AB, Edwards AM, Smiley JR. Herpes simplex virus triggers and then disarms a host antiviral response. *J Virol.* 2001;75:750-758.
24. Kanangat S, Babu JS, Knipe DM, Rouse BT. HSV-1-mediated modulation of cytokine gene expression in a permissive cell line: selective upregulation of IL-6 gene expression. *Virology.* 1996; 219:295-300.
25. Roberts ES, Burudi EM, Flynn C, et al. Acute SIV infection of the brain leads to upregulation of IL6 and interferon-regulated genes: expression patterns throughout disease progression and impact on neuroAIDS. *J Neuroimmunol.* 2004;157:81-92.
26. Unsal E, Aksaray S, Koksal D, Sipit T. Potential role of interleukin 6 in reactive thrombocytosis and acute phase response in pulmonary tuberculosis. *Postgrad Med J.* 2005;81:604-607.
27. Gao W, Thompson L, Zhou Q, et al. Treg versus Th17 lymphocyte lineages are cross-regulated by LIF versus IL-6. *Cell Cycle.* 2009;8: 1444-1450.
28. Galiano M, Liu ZQ, Kalla R, et al. Interleukin-6 (IL6) and cellular response to facial nerve injury: effects on lymphocyte recruitment, early microglial activation and axonal outgrowth in IL6-deficient mice. *Eur J Neurosci.* 2001;14:327-341.
29. Beyer CF, Hill JM, Reidy JJ, Beuerman RW. Corneal nerve disruption reactivates virus in rabbits latently infected with HSV-1. *Invest Ophthalmol Vis Sci.* 1990;31:925-932.
30. Fenton RR, Molesworth-Kenyon S, Oakes JE, Lausch RN. Linkage of IL-6 with neutrophil chemoattractant expression in virus-induced ocular inflammation. *Invest Ophthalmol Vis Sci.* 2002;43:737-743.
31. Biswas PS, Banerjee K, Kinchington PR, Rouse BT. Involvement of IL-6 in the paracrine production of VEGF in ocular HSV-1 infection. *Exp Eye Res.* 2006;82:46-54.
32. Hayashi K, Hooper LC, Detrick B, Hooks JJ. HSV immune complex (HSV-IgG: IC) and HSV-DNA elicit the production of angiogenic factor VEGF and MMP-9. *Arch Virol.* 2009;154:219-226.
33. Suzuki R, Sakamoto H, Yasukawa H, et al. CIS3 and JAB have different regulatory roles in interleukin-6 mediated differentiation and STAT3 activation in M1 leukemia cells. *Oncogene.* 1998;17: 2271-2278.
34. Brocke-Heidrich K, Kretzschmar AK, Pfeifer G, et al. Interleukin-6-dependent gene expression profiles in multiple myeloma INA-6 cells reveal a Bcl-2 family-independent survival pathway closely associated with Stat3 activation. *Blood.* 2004;103:242-251.
35. Klein C, Wustefeld T, Assmus U, et al. The IL-6-gp130-STAT3 pathway in hepatocytes triggers liver protection in T cell-mediated liver injury. *J Clin Invest.* 2005;115:860-869.
36. Williamson P, Merida I, Gaulton G. Protein and lipid kinase activation cascades in interleukin-2 receptor signalling. *Semin Immunol.* 1993;5:337-344.
37. Pereda MP, Goldberg V, Chervin A, et al. Interleukin-2 (IL-2) and IL-6 regulate c-fos protooncogene expression in human pituitary adenoma explants. *Mol Cell Endocrinol.* 1996;124:33-42.
38. Herblot S, Chastagner P, Samady L, et al. IL-2-dependent expression of genes involved in cytoskeleton organization, oncogene regulation, and transcriptional control. *J Immunol.* 1999;162: 3280-3288.
39. Schmeck B, Moog K, Zahlten J, et al. Streptococcus pneumoniae induced c-Jun-N-terminal kinase- and AP-1 -dependent IL-8 release by lung epithelial BEAS-2B cells. *Respir Res.* 2006;7:98.
40. Wegrzyn P, Jura J, Kupiec T, et al. A search for genes modulated by interleukin-6 alone or with interleukin-1beta in HepG2 cells using differential display analysis. *Biochim Biophys Acta.* 2006;1762: 319-328.
41. Ono M. Molecular links between tumor angiogenesis and inflammation: inflammatory stimuli of macrophages and cancer cells as targets for therapeutic strategy. *Cancer Sci.* 2008;99:1501-1506.